February 2012

Ph.D. Dissertation

Molecular Modeling Study of JNK1 Inhibitors

Graduate School of Chosun University

Department of Bio-New Drug development

Madhavan Thirumurthy

Molecular Modeling Study of JNK1 Inhibitors

JNK1 억제제의 분자모델링 연구

24th February 2012

Graduate School of Chosun University

Department of Bio-New Drug development

Madhavan Thirumurthy

Molecular Modeling Study of JNK1 Inhibitors

Advisor: Prof. Seung Joo Cho

This dissertation is submitted to the Graduate School of the Chosun University in partial fulfillment of the requirements for the degree of Doctor of Philosophy in science

October 2011

Graduate School of Chosun University

Department of Bio-New Drug development

Madhavan Thirumurthy

This is to certify that the Ph.D. dissertation of Madhavan Thirumurthy has successfully met the dissertation requirements of Chosun University.

Chairman : Prof. Honglae Sohn .....

Committee Member: Prof. Song Yub Shin .....

Committee Member: Prof. Sung Haeng Lee .....

Committee Member: Prof. Eun Ae Kim .....

Committee Member: Prof. Seung Joo Cho .....

November 2011

Graduate School of Chosun University

TABLE OF CONTENTS

LIST OF TABLES

LIST OF FIGURES

초 록

JNK1 억제제의 분자모델링 연구

마다완티루멀티

지도교수: 조 승 주

생물정보학

조선대학교 대학원

c-Jun N 말단 카이네이즈 (JNK)는 세린, 쓰레오닌 카이네이즈이며 마이토젠에의하여 활성화되는 단백질 카이네이즈의 일종이다 (MAPK). JNK 유사체의 X선 결정구조가 알려져있다. JNK의 대략적인 구성은 MAP 카이네이즈와 유사하다. 특히 ATP가 결합하는 장소의 아미노산 서열은 상동성 90% 이상, 호몰로지 98%이상이다. 따라서 호몰로지 모델링이 유력하다. 이러한 상황에서는 선택성이 대단히 중요하기 때문에, 활성자리를 자세히 연구하는 것이 필요하다. 본 연구에서는 다양한 방법으로 분자를 배열한 다음, CoMFA (Comparative Molecular Filed Analysis)와 CoMSIA (Comparative Molecular Similarity Indices Analysis) 연구를 하였다. 원자-원자의 중접을 이용한 방법으로는 CoMFA의 경우 (q^2=0.646 and r^2=0.983)를 얻었으며, 파머코포아를 이용한 경우에는 CoMFA의 경우 (q^2 = 0.568, r^2 = 0.938) 그리고 CoMSIA의 경우 (q^2=0.670, r^2 = 0.982)의 결과를 얻었다. 또한 x선 결정구조를 이용한 수용체를 template로 활용한 경우에는 리간드의 구조가 수용체속에서 최적화되었다. 이결과, q^2 = 0.605, r^2 = 0.944 (CoMFA) 그리고, q^2 = 0.587, r^2 = 0.863 (CoMSIA)의 결과를 얻었다. CoMFA와 CoMSIA의 contour 지도를 분석해 보면, 페닐 그룹의 양전하를 띈 치환제가 유리하고 피리미딘 고리에는 소수성 그룹이 필요하다고 생각된다. 더구나 NCI 데이다베이스를 활용한 가상검색으로 가능성이 있는 화합물의 구조정보를 얻을 수 있었다. 이는 선택적이고 강력한 JNK1 억제제의 유도체를 얻는데 대단히 중요하다.

ABSTRACT

Molecular Modeling Study of JNK1 Inhibitors

Madhavan Thirumurthy
Advisor: Prof. Seung Joo Cho, Ph.D.
Department of Bio-New Drug development
Graduate School of Chosun University

c-Jun N-terminal Kinases (JNK) are serine threonine protein kinases and members of the mitogen activated protein kinase family (MAPK). The X-ray crystal structures of all three JNK isoforms have been reported. The overall architecture of JNKs is highly similar to that of other MAP kinases. The amino acid sequence identity of the JNK kinases is higher than 90%, with over 98% homology within the ATP binding site. The high homology of the ATP-binding site within JNK's makes it challenging to design isoform specific ATP-site directed inhibitors. Therefore, designing selective ATP, competitive JNK (1, 2, and 3) inhibitors is still a challenging task. As selectivity is the major issue, our in silico analysis might be the starting point for the synthesis of highly potent and selective JNK1 analogs, and this prompted us to initiate the analysis. The main aim of our study was to optimize the reported selective JNK1 inhibitors (4-anilinopyrimidine derivatives), using three-dimensional quantitative structure activity relationship (3D-QSAR) methods, and also to identify new lead compounds using the receptor based pharmacophore. Selectivity is the key issue, pharmacophore generation using receptor-ligand information could be more realistic and selective. In this work, the most popular 3D-QSAR methods such as, comparative molecular field analysis (CoMFA) and comparative molecular similarity indices analysis (CoMSIA) were performed using different alignment methods. The ligand-based atom-by atom matching alignment has produced better values for CoMFA (q^2=0.646 and r^2=0.983), while in CoMSIA it has achieved only lower statistical values. The pharmacophore-based model has produced (q^2 = 0.568, r^2 = 0.938) and (q^2=0.670, r^2 = 0.982) for CoMFA and CoMSIA models, respectively. As the model was based on the receptor-

guided alignment, all the compounds were optimized within the receptor, resulting in q^2 = 0.605 and r^2 = 0.944 for CoMFA, and q^2 = 0.587 and r^2 = 0.863 for CoMSIA. Molecular Dynamic simulation studies suggested that the generated models were consistent with the low energy protein ligand conformation. The CoMFA and CoMSIA contour maps indicated that the substitutions of the electropositive groups in the phenyl ring, and an addition of hydrophobic groups in the pyrimidine ring, are important to enhance the activity of this series. Moreover, the virtual screening analysis against NCI database yields potentials hits and the results obtained would be useful to synthesize selective and highly potent JNK1 analogs.

1. Introduction

The c-Jun N-terminal kinases (c-JNKs) are a subfamily of the mitogen-activated protein kinase (MAPK) group of serine ／ threonine protein kinases. They are activated in response to proinflammatory cytokines tumor necrosis factor-R (TNF-R) and interleukin-1b (IL-1b), as well as by environmental stress including UV irradiation, hypoxia, and osmotic shock (1). Activated JNKs can phosphorylate various substrates, including transcription factors such as c-Jun, ATF-2, Elk1, NFAT, and p53, which in turn regulate gene expression in eukaryotic cells, as well as nuclear hormone receptors and nonnuclear substrates (2). Accordingly, JNKs are critical regulators of many physiological and pathological processes and involved in many diseases such as ischemic stroke, Parkinson's disease, Alzheimer's disease, inflammatory diseases, obesity and diabetes, cardiovascular disease, and so on (3). In mammalian cells, there are 10 different isoforms of JNKs encoded by three distinct genes – Jnk1, Jnk2, and Jnk3 (4). JNK1 and JNK2 are widely expressed in a variety of human tissues. On the contrary, JNK3 is restricted primarily to the brain, heart, and testis (4, 5). Each JNK isoform has been shown to bind to their substrates with different affinities (4), associating with different diseases mentioned above (3). This variably localized expression, together with the activation by different biochemical pathways, indicates that different JNK isoforms have distinct biological functions.

In recent studies, JNK-1, often in concert with JNK-2, has been suggested to play a central role in the development of obesity-induced insulin resistance which implies therapeutic inhibition of JNK1 may provide a potential solution in type-2

diabetes mellitus (4). JNK2 has been described in the pathology of autoimmune disorders such as rheumatoid arthritis and asthma, and it also has been implicated to play a role in cancer, as well as in a broad range of diseases with an inflammatory component. JNK3 has been shown to play important roles in the brain to mediate neurodegeneration, such as beta amyloid processing, Tau phosphorylation and neuronal apoptosis in Alzheimer's disease, as well as the mediation of neurotoxicity in a rodent model of Parkinson's disease. Therefore, design of selective JNKs inhibitors has gained increasing interest.

Type 2 diabetes is a metabolic disorder that accounts for 120 million patients worldwide and the number is likely to grow to greater than 366 million by the year 2030 (6). Patients with type 2 diabetes are insulin resistant, a condition in which the body fails to respond to insulin properly. JNK1 has recently emerged as an attractive target for diabetes therapy, since JNK1 is believed to play a key role in linking obesity and insulin resistance (7-10). JNK1 disrupts the insulin signaling cascade via phosphorylation of the insulin receptor substrate (IRS-1) at Ser307, which leads to the degradation of IRS-1. JNK1 mice show marked reduction in both plasma glucose and insulin concentrations relative to their wildtype littermates, and thus are protected from diet-induced obesity (8). In addition, JNK1 activity is elevated in adipocytes of type 2 diabetic patients (11). Inhibitors of JNK1 can potentially increase insulin sensitivity, and therefore could be useful as therapeutics for the treatment of type 2 diabetes. Therefore, identifying JNK1 selective inhibitor may contribute towards new methods of

treatment for type 2 diabetes, with reduced side effect risks, and will support further understanding of the roles of individual JNK kinases.

In recent years, a number of JNK inhibitors have appeared in the patent and primary literatures (12-25). Compound classes that have shown good JNK selectivity include: aminopyrazoles, aminopyridines, pyridine carboxamides, benzothien-2-yl-amides and benzothiazol-2-yl acetonitriles, quinoline derivatives, and aminopyrimidines. For a recent review of all these classes see LoGrasso and Kamenecka (26). Most of these classes of compounds did not demonstrate good brain penetration, although Kamenecka et al. recently reported aminopyrimidines showing excellent brain penetration properties (27). Keeping these factors in the mind we choose novel dataset to perform our in silico studies. Recently, Liu et al. (28) reported a novel series of 4-anilinopyrimidine derivatives as JNK1 inhibitors, based on a potent compound identified from high-throughput screening and showed high selectivity over five other closely related MAP kinase, p38, ERK2, AKT1, CHK1, and PAK4.

The X-ray crystal structures of all three JNK isoforms have been reported. The overall architecture of JNKs is highly similar to that of other MAP kinases, such as ERK2 and p38, consisting of an N-terminal domain with mostly β strands, a predominantly R helical C-terminal domain, and a deep cleft between the N and C domains, that comprises the ATP-binding site. The amino acid sequence identity of the JNK kinases is higher than 90%, with over 98% homology within the ATP binding site. The high homology of the ATP-binding site within JNK's makes it challenging to design isoform specific ATP-site directed inhibitors. Therefore, designing selective

ATP, competitive JNK (1, 2, and 3) inhibitors is still a challenging task and the recent review by Siddiqui and Reddy stressed the importance of selectivity (29). As selectivity is the major issue, our in silico analysis might be the starting point for the synthesis of highly potent and selective JNK1 analogs, and this prompted us to initiate the analysis. The main aim of our study was to optimize the reported selective JNK1 inhibitors (4-anilinopyrimidine derivatives), as presented by Liu and coworkers, using 3D-QSAR methods, and also to identify new lead compounds using the receptor based pharmacophore. Since selectivity is the key issue, pharmacophore generation using receptor-ligand information would be more realistic and selective.

As an important technology and tool for drug design, computer-aided drug design methods have been applied to the discovery and design of JNK1 inhibitors. Computational approaches like structure- and ligand-based methodology have been found to be valuable in further optimization and the development of novel inhibitors. Ligand-based three dimensional quantitative structure-activity relationship (3D-QSAR) approaches, including comparative molecular field analysis (CoMFA) (30) and comparative molecular similarity indices analysis (CoMSIA) (31), were reported to be effective for understanding the structure-activity relationships (32). The combination of various QSAR techniques such as Quantum QSAR, hologram QSAR, CoMFA, and CoMSIA have proven the quite successful role in the modern drug discovery (33-37). The 3D-QSAR modeling is useful to predict the activity of new molecules to be synthesized. 3D-QSAR methods serve as an important complement to the structure-based methods. CoMFA and CoMSIA are two 3D-QSAR methods that have been

successfully employed in drug design (38). These methods were useful in the lead optimization and also in understanding the drug-target interaction (39-41). In CoMFA, the biological activity of molecules is correlated with their steric and electrostatic interaction energies. The steric and electrostatic interaction energies are calculated using Lennard- Jones and Coulombic potentials, respectively. In CoMSIA, a distance-dependent Gaussian-type functional form has been introduced, which can avoid singularities at the atomic positions and the dramatic changes of potential energy for those grids in the proximity of the surface. Meantime, no arbitrary definition of cutoff limits is required in CoMSIA. The unique differences between conventional CoMFA and CoMSIA are the field type and the potential function. In CoMSIA, similarity is expressed in terms of different physicochemical properties: steric occupancy, partial atomic charges, local hydrophobicity, and H-bond donor and acceptor properties. Moreover, in CoMSIA, a Gaussian-type distance-dependent function has been used to calculate different kinds of physicochemical properties. The unique differences between conventional CoMFA and CoMSIA are the field type and the potential function. Both 3D-QSAR methods give contour maps as output that can be used to get some general insights into the topological features of the binding site.

In the present work, we report the 3D-QSAR study on JNK1 inhibitors, using CoMFA CoMSIA techniques, to find their common structural features. Our work deals with receptor-guided, as well as ligand-based techniques, which include atom-by atom matching and pharmacophore schemes, to generate reasonable CoMFA and CoMSIA models. First, we applied a ligand-based strategy, using the systematic conformation

method, and another ligand-based alignment was performed using the pharmacophore technique with the GALAHAD (Genetic Algorithm with Linear Assignment of Hypermolecular Alignment of Datasets) module in Sybyl8.1. The 3D-QSAR model was obtained from receptor-guided techniques, using available X-ray crystal structure. In addition, we also applied the molecular dynamics (MD) simulation method, to compare the binding mode with the 3D-QSAR model. Finally, CoMFA and CoMSIA contour plots were utilized to elucidate the structural requirement to improve the potency of reported selective JNK1 analogs. Furthermore, a receptor based pharmacophore query was generated by using the complex structure of JNK1 inhibitors. The generated 3D pharmacophoric query was submitted to the NCI database to identify new hits. The hit compounds will be subsequently subjected to filtering by Lipinski's rule of five (42) and docking studies to refine the retrieved hits. Finally, the docking experiments have also been performed with the aim of elucidating the possible binding mode of these identified hit compounds. We expect that our theoretical results would give some useful reference for the researchers in the design of novel and selective JNK1 inhibitors.

2. Materials and Methods

2.1 Inhibitor data set

Series design refers to the process of selecting a set of compounds to be included in a study, with the aim of gaining maximum amount of information possible with a minimum number of compounds. The selection of subset of compounds that represent the total set is important not only in series design, but also in the selection of compounds for training set in 3D-QSAR analysis. CoMFA and CoMSIA model from a well-designed set of compounds is expected to improve the interpretability and the predictiveness of a CoMFA and CoMSIA model. In 3D-QSAR one should utilize accurate activity data in order to develop a good model. Though 3D-QSAR methods can be applied to heterogeneous data sets, some considerations for maintaining the accuracy of biological data are necessary:

• Compounds should belong to a congeneric series (more important in case of classical QSAR). • Compounds should have the same mechanism of action and same/comparable binding mode. • The biological activities of compounds should correlate to their binding affinity and their enumerated biological responses should be measurable.

• Biological data for molecules should be obtained using uniform protocols (radioligand, activator, cofactor, pH, buffer *etc*.) and preferably from a single source (organism/tissue/cell/protein) and single lab.

• Activity data for all the compounds should be in same units of measurement (binding/functional/IC50/*Ki*).

• The ranges of biological activity covered should be as large as possible, keeping the mode of action identical. Preferably, activity range should be much larger than the standard deviations of the data; more than three logarithm units with an even spread of data is preferred.

For our research work, the above important considerations were kept in mind while selecting the biological data set. The structures of the 4-anilinopyrimidines derivatives and their biological activities of thirty five compounds were taken from the literature (28). All original IC_{50} values, of each inhibitor, were converted into pIC_{50} ($-\log IC_{50}$), in order to use the data as the dependent variable in both CoMFA and CoMSIA models. The test set molecule is the truly representative molecule for training set molecules. The test set molecule should cover all the biological activity which is similar to the training set molecule. The total set of compounds was divided into a training set, consisting of 29 compounds, and a test set, consisting of 6 compounds. The selection of both training and test sets was done manually, so that low, moderate, and high JNK inhibitory activities were all represented. The training set was used to build predictive models, while the test set was used to validate the predictive ability of the models. The activities of molecules in the prediction set were predicted in the

present work. The structures and their biological activity values are displayed in Table 1.

Table 1. Structures and biological activities (pIC_{50}) of JNK1 inhibitors.

Table 1. Structures and biological activities (pIC_{50}) of JNK1 inhibitors.

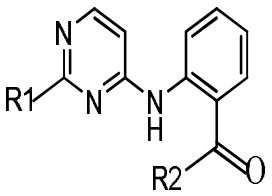

Compound 1-8

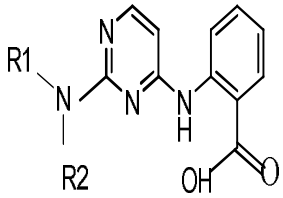

Compound 9-12

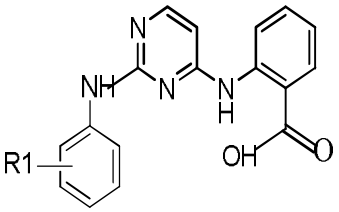

Compound 13-26

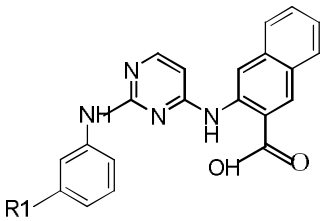

Compound 27-28

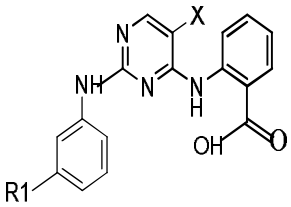

Compound 29-32

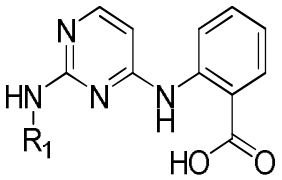

Compound 33-35

Compound No	R1	R2	X	pIC_{50}
1	OBu	OH	-	5.721
2	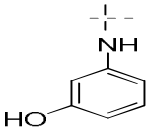	NH_2	-	8.046
3*	OEt	OH	-	4.350
4	OPr	OH	-	5.638
5	OPentyl	OH	-	5.959
6	O-i-Bu	OH	-	6.155
7	O-CH2-c-Hex	OH	-	6.155
8	OPh	OH	-	6.523
9	Bu	H	-	5.585
10	Bn	H	-	4.740
11	c-Hex	H	-	6.398
12	$-(CH2)_6-$	H	-	4.812
13*	H	-	-	7.319
14	2-OH	-	-	7.119
15	3-OH	-	-	7.602
16	4-OH	-	-	7.456
17	2-F	-	-	7.456
18	3-F	-	-	7.553
19	4-F	-	-	7.538
20*	3-Me	-	-	6.804
21	3-F,4-Me	-	-	7.032
22	2-Me,3-OH	-	-	6.556
23	3-CF3	-	-	6.408
24	4-CF3	-	-	6.730
25*	4-NO2	-	-	7.481

26	4-Morpholine	-	-	7.432
27	H	-	-	6.152
28	OH	-	-	6.690
29*	H	-	F	7.086
30	OH	-	F	7.678
31	H	-	Br	7.495
32	OH	-	Br	7.699
33	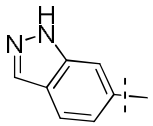	-	-	7.337
34	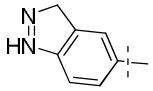	-	-	7.260
35*	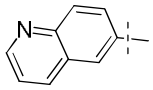	-	-	7.071

***Test set compounds**

2.2 Preparation of the protein structure

The complex structure of the JNK1 protein was retrieved from the protein data bank (PDB code 2NO3) and prepared for receptor by using the protein preparation tool in the Sybyl Biopolymer module. All water molecules were removed and hydrogen atoms were added to the molecule. Energy minimization of hydrogen atoms, followed by energy minimization of side chains, keeping the backbone fixed, was carried out using both simplex and Powell conjugate gradient algorithms, until a gradient of 0.05 kcal/mol was reached. All minimization steps were performed using the Tripos force field within the Sybyl8.1 molecular modeling package (43).

2.3. 3D-QSAR studies: CoMFA and CoMSIA

CoMFA and CoMSIA have proven a very useful 3D-QSAR technique in the field of medicinal chemistry, as indicated by many publications over the past years (44-138). 3D-QSAR methods are an important complement to structure-based affinity prediction methods. If one already has a series of molecules and their corresponding binding affinities, then a 3D-QSAR equation may provide a valuable method to forecast affinity of further analogs. Knowledge of the structure of the binding site would guide the molecular modeling and should prevent unwarranted extrapolation of equations. The 3D-QSAR methods focus on the following goals; (i) to quantitatively correlate and recapitulate the relationships between trends in chemical structure alterations and respective changes in biological endpoint for comprehending which chemical properties are most likely determinants for their biological activities, (ii) to optimize the existing leads so as to improve their biological activities, (iii) to predict the biological activities of untested and sometimes yet unavailable compounds.

Several factors influence the modeling results of CoMFA and CoMSIA: among them, the most important are alignments and fields. Molecular alignment is a prelude to CoMFA and CoMSIA (139). It was assumed that each molecule binds into the active site in a similar mode, since these compounds share a common scaffold. So that the molecules were aligned in a common orientation relative to a template compound in order to compare the different features of analogues. A CoMFA field is then generated by creating a grid around molecules and calculating the steric and electrostatic potential at each point on the grid using a charged probe atom. In CoMFA

and CoMSIA studies, the position of a molecule is important because the descriptors are calculated based on the coordinates of atoms, hence, different methods of alignment will give different results. There are three main different procedures proposed for aligning molecules for QSAR: substructure overlap, pharmacophore overlap and receptor-based alignment. In the present work, we performed different alignment methods, in order to find the most effective alignment to this dataset.

2.3.1 Ligand based alignment

This method involves corresponding atom to atom pairing between the molecules. It is also called as the pharmacophore approach and is the most popular method, because it gives the best matching of the preselected atom positions. It is beneficial in identifying dissimilarity between similar molecules, but cannot be applied to molecules with different structural types where corresponding atoms are difficult to select. In the ligand based alignment, the most active molecule was used as template. All rotatable bonds were searched with incremental dihedral angle from 120°, using the systematic search conformation method. Conformational energies were computed with electrostatic term, and the lowest energy conformer was selected as template molecule. Then the template was modified for other ligands of the series. The common moiety was constraint for each molecule and only the varying parts were energy minimized by Tripos force field with Gasteiger-Huckel charge, using the conjugate gradient method, and the convergence criterion was 0.05 kcal/mol at 10,000 iteration. The minimized structures were aligned over the template using the atom fit option in Sybyl, and

subsequently, this alignment was used for CoMFA and CoMSIA analysis. The aligned molecules are represented in Figure1 (a).

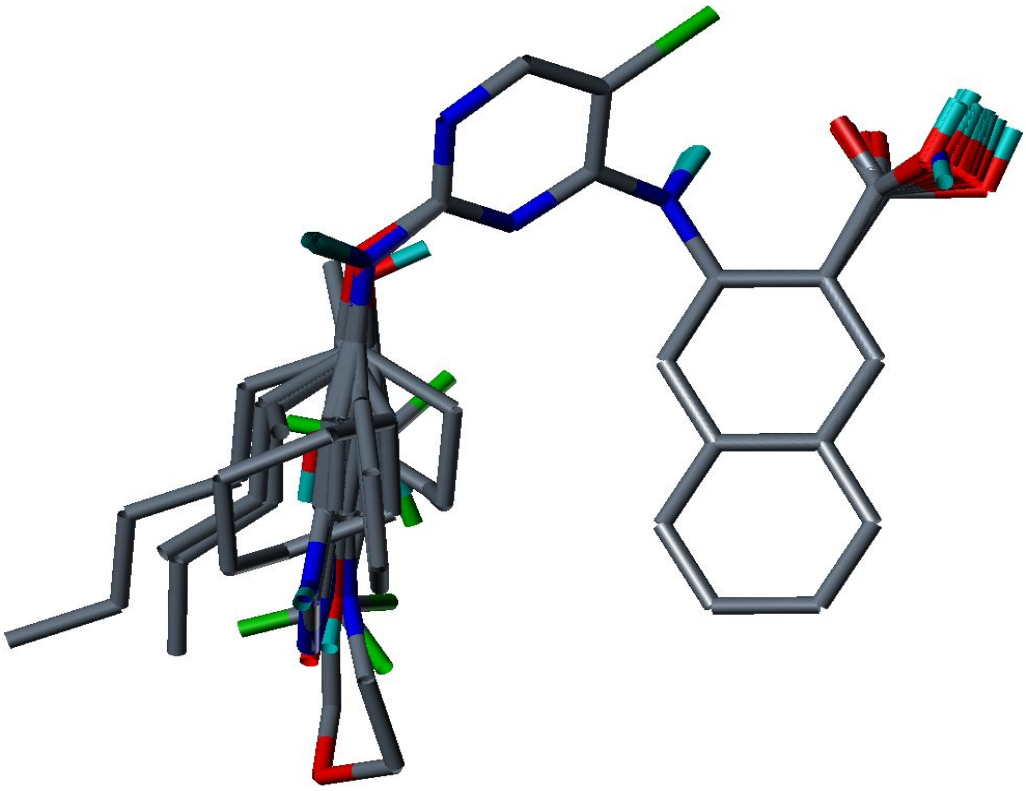

Figure 1 (a): Alignment of 35 studied molecules using atom-by-atom matching.

2.3.2 Pharmacophore based alignment

This method uses a hypothetical pharmacophore as a useful common target template. Each molecule is conformationally directed to assume the shape obligatory for its sub-molecular features to match with either a known pharmacophore or the one which is generated during the conformational analysis. The pharmacophore model was generated with seven highly active inhibitors, using GALAHAD, which is implemented in Sybyl. The program uses the genetic algorithm to generate the pharmacophore hypothesis and the alignments from sets of ligand molecules that bind at a common target site. In the alignment phase, GALAHAD uses a new method, where each molecule is compared with each other, hence there is no template required for model generation. Based on the pharmacophore model, the rest of the compounds were aligned and consequently used for CoMFA and CoMSIA analysis. The pharmacophore model and the alignment of all molecules were presented in Figure 1 (b).

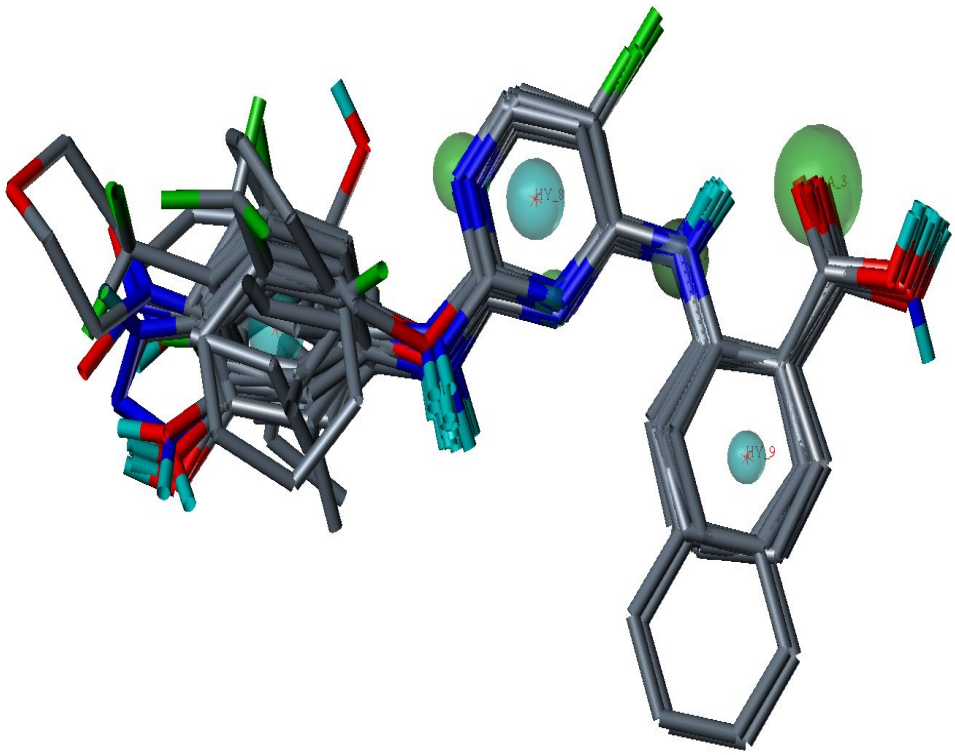

Figure 1 (b): Alignment of 35 studied molecules using pharmacophore features.

2.3.3 Receptor-guided alignment

In this method, molecular alignment is obtained by superimposing the receptor active sites or the receptor residues that interact with the ligands. This approach is believed to be more conceivable, despite problems in conformational analysis due to enhanced degrees of freedom. For receptor-guided alignment, one of the potent inhibitors (i.e. compound 02) was docked into the receptor binding site. The selected conformation served as template to design other ligands. During the energy minimization, both receptor and common moiety of the ligand was restrained, and only the varying parts were minimized within the receptor structure. Gasteiger-Huckel partial atomic charges and Powell's conjugate gradient method were used for minimization of molecules, with the 0.05 kcal/mol energy gradient convergence criterion. All minimized structures were aligned over the template molecule and directly used for CoMFA and CoMSIA. The superimposed inhibitors are shown in Figure 1 (c).

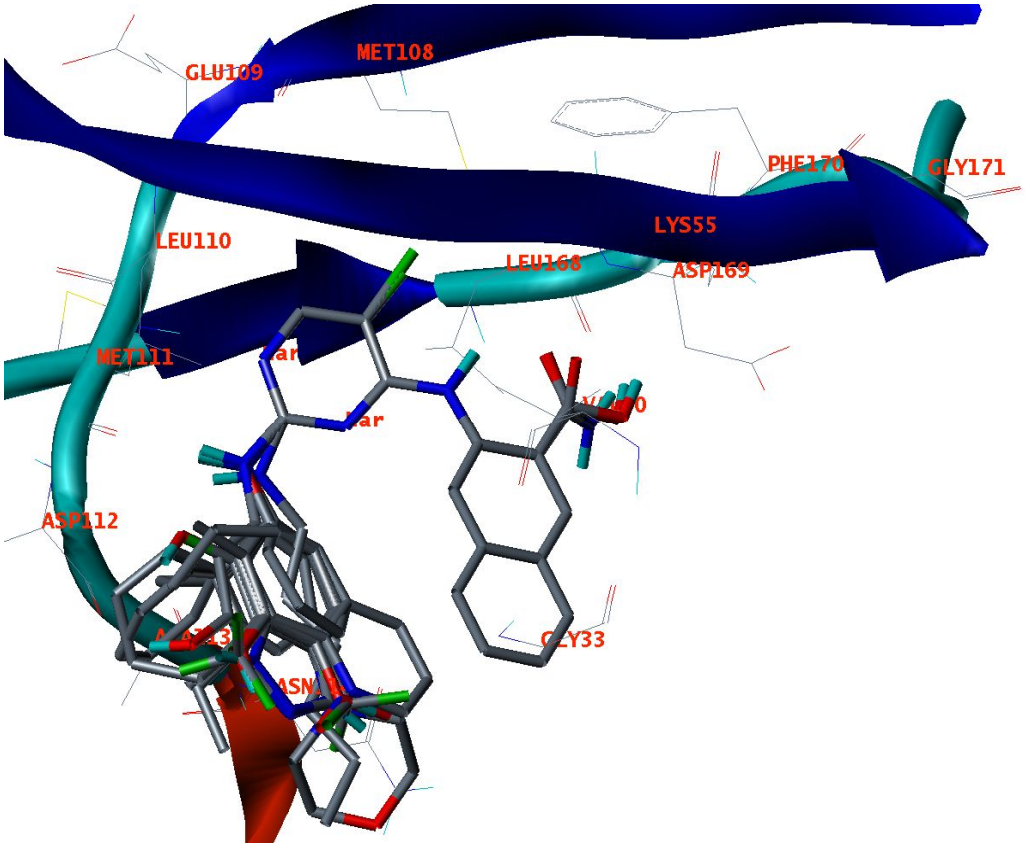

Figure 1 (c): Alignment of 35 studied molecules using receptor –guided method.

2.4. CoMFA model calculation

In 1987, Cramer developed the predecessor of 3D approaches called Dynamic Lattice-oriented molecular modeling system (DYLOMMS) that involves the use of PCA to extract vectors from the molecular interaction fields which are then correlated with biological activities. Soon after he modified it by combining the two existing techniques, GRID and PLS, to develop a powerful 3D-QSAR methodology, Comparative Molecular Field Analysis (CoMFA). Today CoMFA has become a prototype of 3D-QSAR methods. A standard CoMFA procedure, as implemented in the Sybyl Software from Tripos Inc.

In this work, we used Sybyl8.1 molecular modeling package to generate CoMFA model. CoMFA calculations were carried out by applying the default settings. The aligned molecules were placed in the 3D cubic lattice, with the grid spacing of 1.0-2.0Å. The standard CoMFA field performed the Lennard-Jones potential and the Coulombic potential, for the steric and electrostatic fields, respectively. The cut off value for both fields was set to 30 kcal/mol. Steric and electrostatic energies were calculated using the sp^3 carbon atom, with van der Waal's radius of 1.52Å and +1 charge, at each lattice point.

2.5. CoMSIA model calculation

Comparative Molecular Similarity Indices Analysis (CoMSIA) was developed to overcome certain limitations of CoMFA. In CoMSIA, molecular similarity indices calculated from modified SEAL similarity fields are employed as descriptors to

simultaneously consider steric, electrostatic, hydrophobic and hydrogen bonding properties. These indices are estimated indirectly by comparing the similarity of each molecule in the dataset with a common probe atom (having a radius of 1 Å, charge of +1 and hydrophobicity of +1) positioned at the intersections of a surrounding grid/lattice. For computing similarity at all grid points, the mutual distances between the probe atom and the atoms of the molecules in the aligned dataset are also taken into account. To describe this distance-dependence and calculate the molecular properties, Gaussian-type functions are employed. Since the underlying Gaussian-type functional forms are 'smooth' with no singularities, their slopes are not as steep as the Coulombic and Lennard-Jones potentials in CoMFA; therefore, no arbitrary cut-off limits are required to be defined. These functions tend to produce values within a reasonable range, even in the case of overlapping atoms. CoMSIA similarity indices (A_F) for molecule j with atoms i at a grid point q were calculated using the following Eq.

Where k represents the following physicochemical properties: steric, electrostatic, hydrophobic, H-bond donor and H-bond acceptor. A Gaussian type distance dependence was used between grid point q and each atom i of the molecule. The default value of 0.3 was used as the attenuation factor (α). The steric indices were related to the third power of the atomic radii, electrostatic descriptors are derived from atomic partial charges, hydrophobic fields were derived using atom-based parameters (140) and H-bond donor and acceptor indices were obtained by a rule-based method based on

experimental results (141). CoMSIA analyses were performed with all possible descriptors' combinations which is similar to the one reported by Teixeira et al. (142).

2.6. Statistical method used for building 3D-QSAR model: Partial least square (PLS):

The relationship between the structural parameters and the biological activities has been quantified by the PLS algorithm (143, 144). It is an iterative regression procedure that produces its solutions based on linear transformation of a large number of original descriptors to a small number of new orthogonal terms called latent variables (145). PLS gives a statistically robust solution even when the independent variables are highly interrelated among themselves, or when the independent variables exceed the number of observations. Thus, PLS is able to analyze complex structure-activity data in a more realistic way, and effectively interpret the influence of molecular structure on biological activity. This is one of the standard statistical methods used for the development of predictive 3D-QSAR models.

2.7. Validation of QSAR models:

PLS methodology, which is an extension of multiple regression analysis, was used for the 3D-QSAR in which the independent variables were the CoMFA and CoMSIA descriptors, and $p\text{IC}_{50}$ values were used as dependent variables. Before the PLS analysis, the CoMFA and CoMSIA columns were filtered by using column filtering. The best 3D-QSAR models generated from the PLS analysis, ranked

according to their coefficient of determination (or squared correlation coefficient) (r^2) values, were submitted to a standard internal validation technique, named 'leave-one-out' cross-validation (LOO-CV), that gives the LOO-CV r^2 (q^2) as a statistical index of predictive power. In the LOO-CV procedure, the coefficients of the independent variables of the original PLS model are recalculated, excluding one compound (i.e., activity values and calculated properties) from the original training set at once, and this 'new' model is used to predict the activity of the excluded compound. This procedure is repeated through the whole data set, until all compounds have been excluded once, and then, q^2 values and standard error of predictions (SEP) are calculated. The cross-validated coefficient q^2 (or r^2_{cv}) was evaluated as:

$$q^2 = 1 - \frac{\sum_{\gamma} (\gamma_{pred} - \gamma_{actual})^2}{\sum_{\gamma} (\gamma_{actual} - \gamma_{mean})^2}$$

where $\gamma_{predicted}$, γ_{actual}, γ_{mean} are the predicted, observed, and mean values of the pIC_{50}, respectively. After the predictive quality of the best correlation model is determined, the optimum number of components is employed to perform a non validation PLS analysis with the same column filtering set to get the final model.

The CoMFA/CoMSIA results were graphically represented by field contour maps, where the coefficients were generated using the field type 'StDev*Coeff'. In order to test the real predictive ability of the best models generated by the 3D-QSAR CoMFA/CoMSIA approaches using the training set, the pIC_{50} values of the external validation set were calculate using the same CoMFA/CoMSIA options which generated

the best models, as described before. The quality of the external prediction is documented using the standard deviation of error prediction (r^2_{pred}), according to the below Equation.

$$r^2_{pred} = \frac{(SD - PRESS)}{SD}$$

In the equation , PRESS is the sum of the squared deviations between predict and actual pIC_{50} values for the test set compounds and SD is the sum of the squared deviation between the actual pIC_{50} values of the compounds in the test set and the mean pIC_{50} value of the training set compounds.

2.8. Molecular dynamics

Molecular dynamics study was carried out to compare the binding mode of the protein-ligand complex with the 3D-QSAR model. All molecular simulation was performed using the GROMACS 4.0.7 software (146). The PRODRG (147) server was used to build the Gromacs 87 topology for the ligand molecule. The protein complex was placed into the cubic box and then minimized, using the steepest descent algorithm. Periodic boundary conditions were applied in all directions, and the system was neutralized by adding appropriate counter ions (Na^+ or Cl^-). Prior to the simulation, an energy minimization was applied to the full system without constraints using the steepest descent integrator for 9896 steps, then the system was equilibrated via a 200 ps MD simulation at 300 K. Finally, a 2 ns simulation was performed with a time step of 2 fs. During MD simulation, the standard parameters and main calculation methods were

set as follows: The model used NPT ensemble at 300 K with periodic boundary conditions, the temperature was kept constant by the Berendsen thermostat, the values of the isothermal compressibility were set to 4.5×10^{-5} bar^{-1} while the pressure was maintained at 1 bar using the Parrinello-Rahman scheme (148), electrostatic interactions were calculated using the particle mesh Ewald method (149,150), and cutoff distances for the calculation of Coulomb and van der Waals interactions were 1.0 and 1.4 nm, respectively. All the MD simulations lasted 2 ns to ensure that the whole systems were stable. Snap shots were collected at every 1 ps and subsequent analyses were performed using the GROMACS tools.

2.9. 3D Pharmacophore search

Pharmacophore is an important and unifying concept in rational drug design that embodies the notion that molecules are active at a particular enzyme or receptor because they possess both a number of chemical features that favor the target interaction and geometry complementary to it (151). A pharmacophore hypothesis collects common features distributed in three-dimensional space representing groups in a molecule that participate in important interactions between drug and active site. Pharmacophore model provides a rational hypothetical picture of the primary chemical features responsible for activity. Since the last few years pharmacophore modeling has been one of the important and successful approaches for new drug discovery (151-153). Particularly, the 3D pharmacophore searching is extremely useful to identify new lead compounds that have the desired activity but which are from a previously unexplored

chemical series. It depends on the atomic properties rather than element type. In our work, we performed spatial and partial match constraint method to generate the 3D-pharmacophore query on the basis of the crystal structure bound conformation. By utilizing this complex structure, pharmacophore query was generated for donor and acceptor site of receptor. The 3D pharmacophore search was performed using the Unity flexible search protocol with all options set as default against the National Cancer Institute 3D database (NCI2000), and it contains approximately 2×10^5 compounds. In the unity query search, the conformations of the screened database were generated on the fly by means of the Directed tweak method (154). The generated query rapidly finds molecules that are guided by the given pharmacophore query, and selected reasonable conformations are stored in a database. Primary screening was carried out by various filtration criteria, such as the Lipinski's Rule of five, the Vander Waals bumps and by restricting the number of rotatable bonds to a maximum of 7. Several hits were identified from the NCI database, which were further refined by using the Surflex docking studies.

2.10. Molecular docking

The Surflex-Dock was applied to carry out receptor-guided alignment based QSAR models Furthermore, it was used to perform the screening and validation of hits obtained from the database searching. Surflex-Dock was reported to be one of the best docking software. Performance of the docking accuracy and screening utility of Surflex is comparable with the best available methods reported in the literature (155, 156). It

implements the Hammerhead's empirical scoring function (157) with the molecular similarity method to create putative poses of ligand fragments. The docking algorithm uses the idealized active site called the protomol (158). A protomol is a computational representation of the intended binding site to which putative ligands are aligned. Two parameters, such as threshold and bloat, determine the extent of a protomol. The threshold factor indicates how much the protomol is buried inside the protein, and the bloat parameter provides a way to increase the protomol volume. The threshold 0.50 and bloat parameter 1 Å were used for protomol generation. The purpose of the protomol is to direct the initial placement of the ligand during the docking process. The protomol was generated based on the ligand inside the active site. Protomols were visualized with Sybyl 8.1 to ensure proper coverage of the desired target area. The docking score was expressed as –log10 (K_d), to represent the binding affinities, and the consensus scoring function was used to rank the affinity of the ligand bound to the active site. Other parameters were employed with the default setting.

3. Results and Discussion

3.1. CoMFA and CoMSIA model analysis (Ligand-based alignment)

The ligand-based CoMFA model was derived with the combination of steric and electrostatic field contribution and Gasteiger-Hückel charge method with different grid space. The Leave one out (LOO) analysis gave the cross-validated q^2 of 0.646 with five components and non cross-validated PLS analysis resulted in a correlation coefficient r^2 of 0.983, F= 273.262, and an estimated standard error of 0.125. We further performed bootstrapping analyses to evaluate the robustness and statistical confidence of the final models (r^2_{boot}= 0.991, StdDev= 0.005). Statistical results obtained from the constructed model verified the predictive ability of the model (Table 2) and further implied that the steric and electrostatic factors contribute to the binding affinities. The predictive ability of the developed CoMFA model was assessed by the test set (six molecules) predictions, which were excluded during CoMFA model generation. The predictive ability of the test set was 0.674.

The CoMSIA models were generated with the different field combinations using Gasteiger-Hückel charge method with 1.0 Å grid space. The combinations of all descriptors such as steric (S), electrostatic (E), hydrophobic (H), hydrogen bond donor (D), and hydrogen bond acceptor (A) were listed in Table 3. The lingad-based model for CoMSIA yielded q^2 = 0.464 and r^2 = 0.651 with n=1. The SEE for CoMSIA model was found to be 0.530. The predictive ability of the developed CoMSIA model was assessed by the test set (six molecules) predictions, which were excluded during CoMSIA model generation. The predictive ability of the test set was 0.318.

Table 2: Statistics summary of CoMFA models using ligand-based alignment method.

Model No	Grid (Å)	Leave-one-out cross-validation			Non-cross-validation			Bootstrap		r^2_{pred}	Field contribution	
		q^2	n	SDEP	r^2	SEE	F-value	r^2_{boot}	StdDev		S	E
1	**1.0**	**0.646**	**5**	**0.578**	**0.983**	**0.125**	**273.262**	**0.991**	**0.005**	**0.674**	**0.544**	**0.456**
2	1.5	0.619	5	0.600	0.985	0.119	301.263	0.990	0.005	-	0.565	0.435
3	2.0	0.605	4	0.598	0.967	0.174	174.287	0.982	0.009	-	0.578	0.422

q^2= cross-validated correlation coefficient; n= number of statistical components; SDEP= standard deviation estimated prediction; r^2= non-cross validated correlation coefficient; SEE=standard estimated error; F=Fisher value; r^2_{boot}=correlation coefficient after 100 runs of bootstrapping; r^2_{pred}= predictive correlation coefficient for test set; S= steric; E= electrostatic.

Table 3: Statistics summary of CoMSIA models using ligand-based alignment method.

Model No.	Field					LOO cross-validation		Non-cross-validation			r^2_{pred}
	S	E	H	D	A	q^2	n	r^2	SEE	F	
1	0.199	0.801	-	-	-	0.431	1	0.606	0.563	41.497	-
2	0.265	-	0.735	-	-	0.440	1	0.627	0.548	45.295	-
3	0.128	0.516	0.356			0.457	1	0.640	0.538	47.958	-
4	0.188	-	0.461	0.351	-	0.427	2	0.824	0.383	61.000	-
5	**0.209**	**-**	**0.578**	**-**	**0.213**	**0.464**	**1**	**0.651**	**0.530**	**50.389**	**0.318**
6	0.117	0.381	0.290	0.507	-	0.460	2	0.838	0.368	67.124	-
7	0.113	0.456	0.315	-	0.116	0.456	1	0.638	0.540	47.553	-
8	0.166	-	0.414	0.298	0.121	0.456	1	0.638	0.387	59.371	-
9	0.109	0.348	0.275	0.194	0.073	0.452	2	0.833	0.374	64.725	-

S =steric field, E = electrostatic field, H =hydrophobic field, D =hydrogen bond donor, A= hydrogen bond acceptor; n= number of statistical components; q^2= cross-validated correlation coefficient; r^2= non-cross validated correlation coefficient; SEE=standard estimated error; F=Fisher value; r^2_{pred}= predictive correlation coefficient for test set.

3.2. CoMFA and CoMSIA model analysis (Pharmacophore-based alignment)

The Pharmacophore-based CoMFA model was derived with the combination of steric and electrostatic field contribution and Gasteiger-Hückel charge method with different grid space. The Leave one out (LOO) analysis gave the cross-validated q^2 of 0.568 with three components and non cross-validated PLS analysis resulted in a correlation coefficient r^2 of 0.938, F= 126.902, and an estimated standard error of 0.231. We further performed bootstrapping analyses to evaluate the robustness and statistical confidence of the final models (r^2_{boot}= 0.954, StdDev= 0.020). Statistical results obtained from the constructed model verified the predictive ability of the model (Table 4) and further implied that the steric and electrostatic factors contribute to the binding affinities. The predictive ability of the developed CoMFA model was assessed by the test set (six molecules) predictions, which were excluded during CoMFA model generation. The predictive ability of the test set was 0.670.

The CoMSIA models were generated with the different field combinations using Gasteiger-Hückel charge method with 1.5 Å grid space. The combinations of all descriptors such as steric (S), electrostatic (E), hydrophobic (H), hydrogen bond donor (D), and hydrogen bond acceptor (A) were listed in Table 5. The pharmacophore-based model for CoMSIA yielded q^2 = 0.670 and r^2 = 0.938 with n=3. The SEE for CoMSIA model was found to be 0.231. The predictive ability of the developed CoMSIA model was assessed by the test set (six molecules) predictions, which were excluded during CoMSIA model generation. The predictive ability of the test set was 0.563.

Table 4: Statistics summary of CoMFA models using pharmacophore-based alignment method.

Model No	Grid (Å)	Leave-one-out cross-validation			Non-cross-validation			Bootstrap		r^2_{pred}	Field contribution	
		q^2	n	SDEP	r^2	SEE	F-value	r^2_{boot}	StdDev		S	E
4	1.0	0.548	3	0.627	0.944	0.220	140.824	0.958	0.021	-	0.469	0.531
5	**1.5**	**0.568**	**3**	**0.613**	**0.938**	**0.231**	**126.902**	**0.954**	**0.020**	**0.670**	**0.401**	**0.549**
6	2.0	0.556	3	0.621	0.951	0.207	160.109	0.958	0.019	-	0.498	0.502

q^2= cross-validated correlation coefficient; n= number of statistical components; SDEP= standard deviation estimated prediction; r^2= non-cross validated correlation coefficient; SEE=standard estimated error; F=Fisher value; r^2_{boot}=correlation coefficient after 100 runs of bootstrapping; $r^2_{predictive}$= predictive correlation coefficient for test set; S= steric; E= electrostatic.

Table 5: Statistics summary of CoMSIA models using pharmacophore -based alignment method.

Model No.	Field					LOO cross-validation		Non-cross-validation			r^2_{pred}
	S	E	H	D	A	q^2	n	r^2	SEE	F	
10	0.167	0.833	-	-	-	0.388	1	0.679	0.508	57.044	-
11	**0.274**	**-**	**0.726**	**-**	**-**	**0.670**	**6**	**0.982**	**0.133**	**202.488**	**0.563**
12	0.146	0.523	0.331	-	-	0.423	2	0.850	0.354	73.888	-
13	0.179	-	0.451	0.370	-	0.539	6	0.986	0.118	257.271	-
14	0.201	-	0.554	-	0.246	0.556	5	0.973	0.161	163.093	-
15	0.107	0.397	0.255	0.247	-	0.482	2	0.852	0.351	75.031	-
16	0.121	0.415	0.303	-	0.160	0.410	2	0.868	0.332	85.613	
17	0.141	-	0.387	0.305	0.163	0.473	4	0.937	0.240	88.531	-
18	0.092	0.334	0.239	0.215	0.120	0.448	2	0.854	0.349	76.076	-

S =steric field, E = electrostatic field, H =hydrophobic field, D =hydrogen bond donor, A= hydrogen bond acceptor; n= number of statistical components; q^2= cross-validated correlation coefficient; r^2= non-cross validated correlation coefficient; SEE=standard estimated error; F=Fisher value; r^2_{pred}= predictive correlation coefficient for test set.

3.3.CoMFA and CoMSIA model analysis (receptor-guided alignment)

For a reliable predictive model, the cross-validation coefficient q^2 should be more than 0.5 (159). Both the ligand-based and the receptor-guided techniques have achieved expected statistical values for CoMFA. The ligand-based atom-by atom matching alignment yielded $q^2 = 0.646$ and $r^2 = 0.983$ values for CoMFA, whereas the pharmacophore alignment produced a slightly lower q^2 value for CoMFA, when compared with other alignment methods (i.e. $q^2 = 0.568$ and $r^2 = 0.938$). The reliable CoMFA model 8 was obtained from the receptor-guided alignment using the combination of steric and electrostatic field descriptors, with the grid spacing 1.5 Å ($q^2 = 0.605$ and $r^2 = 0.944$) (Table 6). A bootstrapped r^2 of 0.971 with the standard deviation (StdDev) of 0.015 were obtained from bootstrapping analysis (100 runs), to further confirm the statistical validity and the robustness of the established CoMFA model. Even though ligand-based model looks superior in statistics, we chose the receptor-guided method to produce the 3D-QSAR model, because it generates more reliable models, with better understanding of the receptor interactions, than the ligand-based alignment.

CoMSIA is an alternative approach to perform 3D-QSAR by comparative molecular field analysis. Molecular similarity is compared in terms of similarity indices. The CoMSIA model was derived, with various combinations of steric, electrostatic, hydrophobic, hydrogen-bond donor and hydrogen-bond acceptor fields. The statistical summary of CoMSIA results indicate that atom-by atom matching

alignment showed lower q^2 values (i.e. q^2 = 0.464 and r^2 = 0.651), than the pharmacophore based alignment (q^2 = 0.670 and r^2 = 0.982). A better CoMSIA model was obtained with the receptor-guided method, combining steric, hydrophobic and hydrogen-bond acceptor fields. The combination of these fields yielded reliable statistical results (i.e. q^2 = 0.587 and r^2 = 0.863) (Table 7). From these field contribution results, we identified that the hydrophobic field played a major contribution in the present series of molecules.

Table 6: Statistics summary of CoMFA models using receptor-guided alignment method.

Model No	Grid (Å)	Leave-one-out cross-validation			Non-cross-validation			Bootstrap		r^2_{pred}	Field contribution	
		q^2	n	SDEP	r^2	SEE	F-value	r^2_{boot}	StdDev		S	E
7	1.0	0.580	4	0.770	0.955	0.201	128.326	0.947	0.016	-	0.595	0.405
8	**1.5**	**0.605**	**4**	**0.792**	**0.944**	**0.224**	**101.781**	**0.971**	**0.015**	**0.615**	**0.592**	**0.408**
9	2.0	0.475	4	0.896	0.933	0.246	83.966	0.965	0.020	-	0.569	0.431

q^2= cross-validated correlation coefficient; n= number of statistical components; SDEP= standard deviation estimated prediction; r^2= non-cross validated correlation coefficient; SEE=standard estimated error; F=Fisher value; r^2_{boot}=correlation coefficient after 100 runs of bootstrapping; r^2_{pred}= predictive correlation coefficient for test set; S= steric; E= electrostatic.

Table 7: Statistics summary of CoMSIA models using receptor-guided alignment method.

Model No.	Field					LOO cross-validation		Non-cross-validation			Predictive R^2
	S	E	H	D	A	q^2	n	r^2	SEE	F	r^2_{pred}
19	0.297	0.703	-	-	-	0.552	3	0.885	0.316	64.185	-
20	0.281	-	0.719	-	-	0.605	2	0.847	0.358	71.946	-
21	0.174	0.449	0.377	-	-	0.541	3	0.893	0.305	69.389	-
22	0.223	-	0.525	0.242		0.547	3	0.865	0.343	53.367	-
23	**0.247**	**-**	**0.599**	**-**	**0.155**	**0.587**	**3**	**0.863**	**0.345**	**52.409**	**0.528**
24	0.159	0.381	0.333	0.127	-	0.537	3	0.896	0.301	71.427	-
25	0.166	0.401	0.364	-	0.069	0.547	3	0.890	0.309	67.398	-
26	0.223	-	0.511	0.176	0.090	0.556	3	0.866	0.341	54.047	-
27	0.158	0.363	0.344	0.099	0.037	0.532	3	0.891	0.308	68.123	-

S =steric field, E = electrostatic field, H =hydrophobic field, D =hydrogen bond donor, A= hydrogen bond acceptor; n= number of statistical components; q^2= cross-validated correlation coefficient; r^2= non-cross validated correlation coefficient; SEE=standard estimated error; F=Fisher value; $r^2_{predictive}$= predictive correlation coefficient for test set.

Table 8: The actual pIC_{50}, predicted pIC_{50} and residual values of all compounds derived from the CoMFA and CoMSIA models by receptor-guided alignment.

No.	pIC_{50}	CoMFA		CoMSIA	
		prediction	Residual	prediction	Residual
1	5.721	5.749	0.028	5.842	0.121
2	8.046	7.821	0.225	8.171	0.125
3*	4.350	5.746	1.396	6.075	1.725
4	5.638	5.897	0.259	6.090	0.452
5	5.959	5.900	0.059	5.862	0.097
6	6.155	6.125	0.030	6.176	0.022
7	6.155	5.998	0.158	5.951	0.204
8	6.523	6.663	0.140	6.928	0.405
9	5.585	5.888	0.303	5.801	0.216
10	4.740	4.911	0.171	5.052	0.312
11	6.398	6.041	0.357	5.990	0.409
12	4.812	4.588	0.224	4.638	0.174
13*	7.319	7.233	0.086	7.015	0.304
14	7.119	7.241	0.122	7.226	0.107
15	7.602	7.387	0.215	7.207	0.395
16	7.456	7.439	0.017	7.256	0.200
17	7.456	7.304	0.152	7.012	0.444
18	7.553	7.343	0.210	7.004	0.549
19	7.538	7.371	0.167	7.024	0.514
20*	6.804	7.329	0.525	6.987	0.183
21	7.032	7.235	0.203	6.972	0.060
22	6.556	7.163	0.607	7.287	0.731
23	6.408	6.592	0.184	7.009	0.601
24	6.730	6.744	0.014	7.050	0.320
25*	7.481	7.139	0.342	7.255	0.226
26	7.432	7.385	0.047	7.527	0.095
27	6.152	6.168	0.016	6.240	0.088
28	6.690	6.355	0.335	6.430	0.260
29	7.086	7.612	0.526	7.132	0.046
30	7.678	7.761	0.083	7.322	0.356
31	7.495	7.552	0.057	7.548	0.053
32	7.699	7.691	0.008	7.737	0.038
33	7.337	7.250	0.087	7.306	0.031
34	7.260	7.365	0.105	7.267	0.007
35*	7.071	7.061	0.010	7.325	0.254

*Test set compounds

To validate both the predictability and accuracy of the models, the predictive correlation coefficient r^2_{pred} was calculated for test data set. In the test set, compound 3 had a residual value of 1.396 and 1.725, indicating large residual values of the model. This is because compound 3 has the lowest pIC_{50} value within its cluster and it was not included in the training set. Although this contradicted our predictions, the structural similarity with other compounds determined us to include this compound in the dataset. The r^2_{pred} values for QSAR models were represented in Table 6 and 7. The receptor-based models produce r^2_{pred} values of 0.615 and 0.528, for CoMFA and CoMSIA, respectively. The actual and predicted activity (from the receptor-guided method) of both CoMFA and CoMSIA models are listed in Table 8. The results showed that the activities predicted by the produced models were in good agreement with the original data, suggesting that those models should have satisfactory predictive value. Figure 2 (a) and (b) shows plots of the predicted vs. actual data by the CoMFA and CoMSIA models.

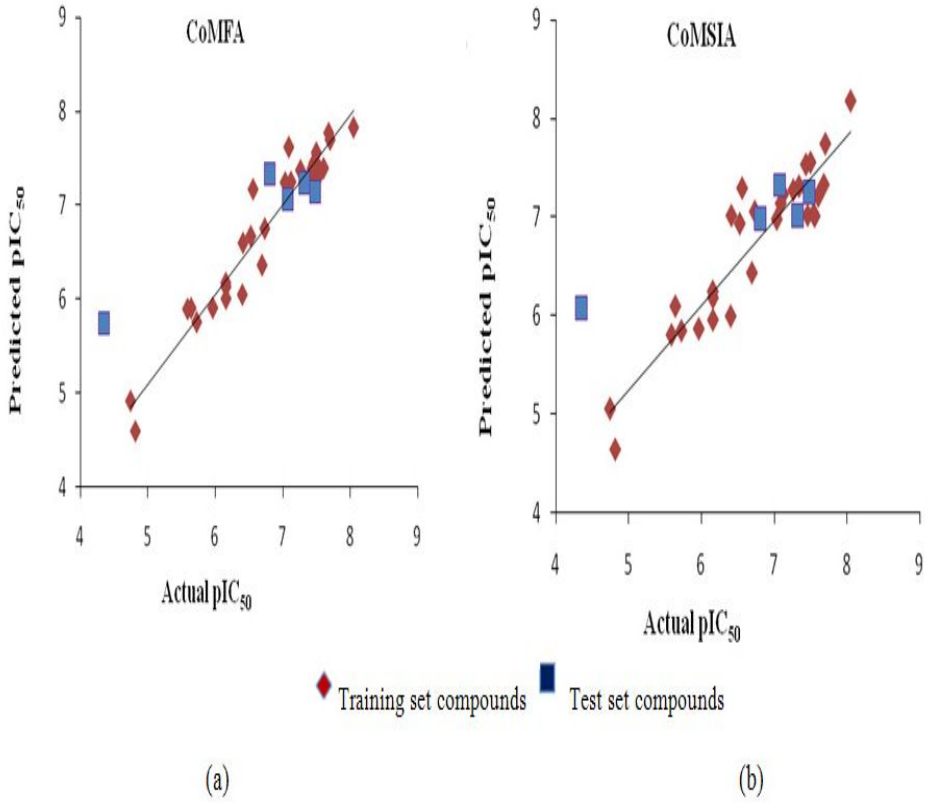

Figure 2: Plot of predicted vs actual values of (a) CoMFA, and (b) CoMSIA (receptor-guided alignment).

3.4. CoMFA contour map (receptor-guided alignment)

The CoMFA contour map was generated based on the receptor-guided alignment method. The CoMFA result is usually represented as a 3D 'coefficient contour' map. It shows regions where variations of steric and electrostatic nature in the structural features of the different molecules contained in the training set lead to either increase or decrease in the activity. The CoMFA steric and electrostatic fields are represented in contour plots. The steric interaction is represented by the green and yellow contours, in which green colored regions indicate areas where increased steric bulk is associated with enhanced activity, and yellow regions suggest areas where increased steric bulk is unfavorable to activity. The electrostatic interaction is indicated by the red and blue contours, in which the blue colored regions show areas where more positively charged groups are favored, and red region highlight areas where groups with more negative partial charges are favored. These contour maps give us some general insight into the nature of the receptor-ligand binding region.

One of the most potent inhibitors, i.e. 02, was superimposed in the active site of the receptor protein. A large favorable steric field (green) is observed around Asp112, Ala113 and Asn114, which are next to the ortho, meta and para positions of the phenyl ring (Figure 3). This indicates that a bulky group at this place is preferred for activity. This result is in agreement with the experimental data showing that compounds 20, 21, 22, 26, 33, 34 and 35 have a bulky substituent in the phenyl moiety and exhibit stronger activities.

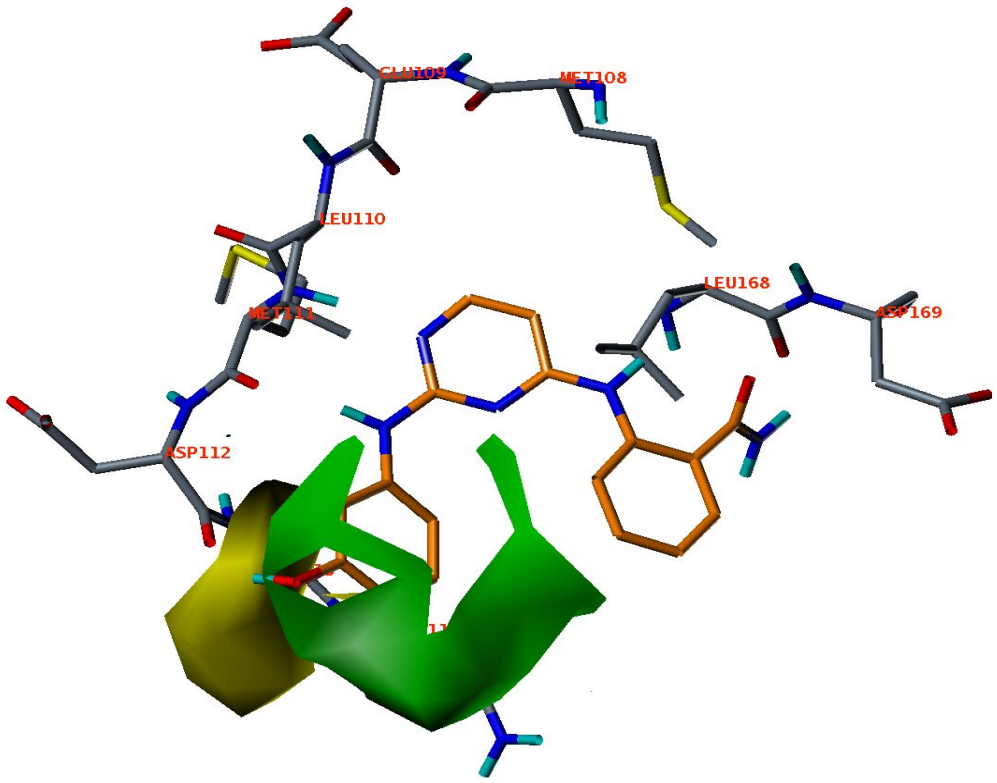

Figure 3: The CoMFA steric contour map with compound 02 (Table 1). Green contours indicate regions where bulky groups increase activity, whereas yellow contours indicate regions where bulky groups decrease activity.

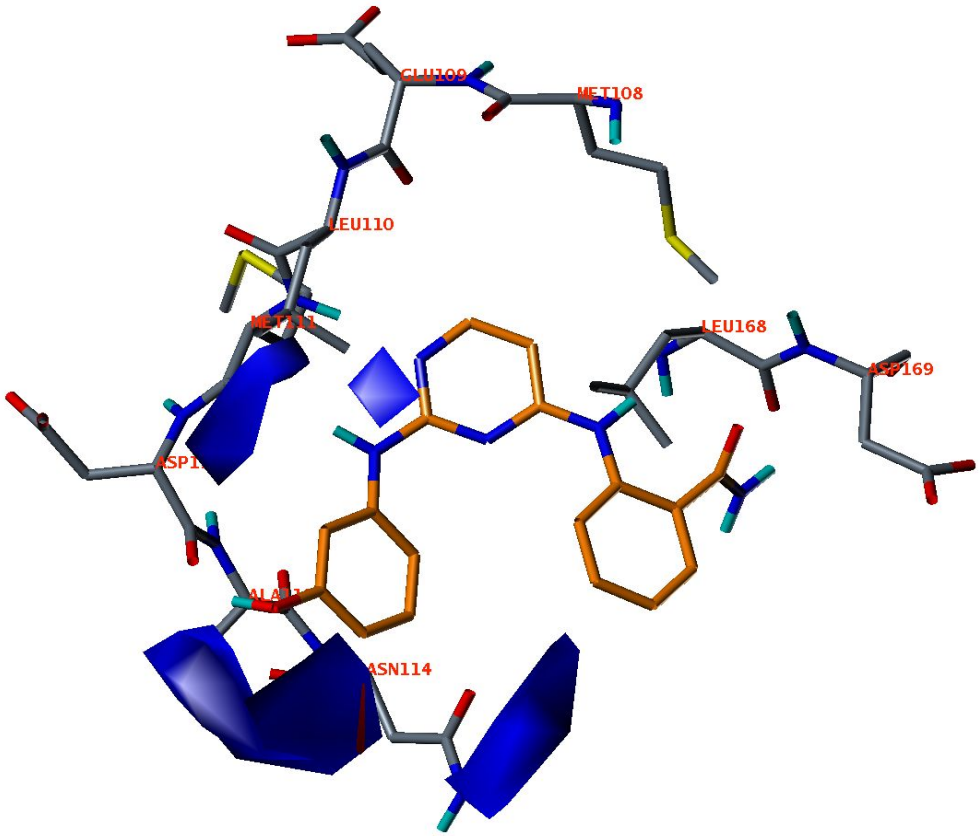

Figure 4: The CoMFA electrostatic contour map with compound 02 (Table 1). Red contours indicate negative charge favoring activity, whereas blue contours indicate positive charge favoring activity.

On the electrostatic contour map (Figure 4) the blue contour region was found close to the NH group of the aniline ring. This positively charged amino group is interacting with the carbonyl group of Met111. Inhibitors 1, 3, 4, 5, 6, 7, and 8 showed that the lower pIC_{50}, which was substituted with the ether group, was unfavorable to the blue contour map. This may be the reason why these compounds show lower biological activity. Another blue contour map was also found close to the meta and para positions of the phenyl ring, indicating that positively charged groups can favorably interact with the surrounding negatively charged backbone residues of both Asp112 and Ala113. This may be the reason why the compounds 2, 14, 15, 16, and 28 show higher biological activity.

3.5. CoMSIA contour map (receptor-guided alignment)

The CoMSIA contour maps were also developed based on the receptor-guided alignment method. Figures 5, 6, and 7 show the steric, hydrophobic and H-bond acceptor contour maps superimposed on the active site of the JNK1. Compared with figure 3, it can be seen that the CoMSIA steric contour map is quite similar to that of the corresponding CoMFA contour map.

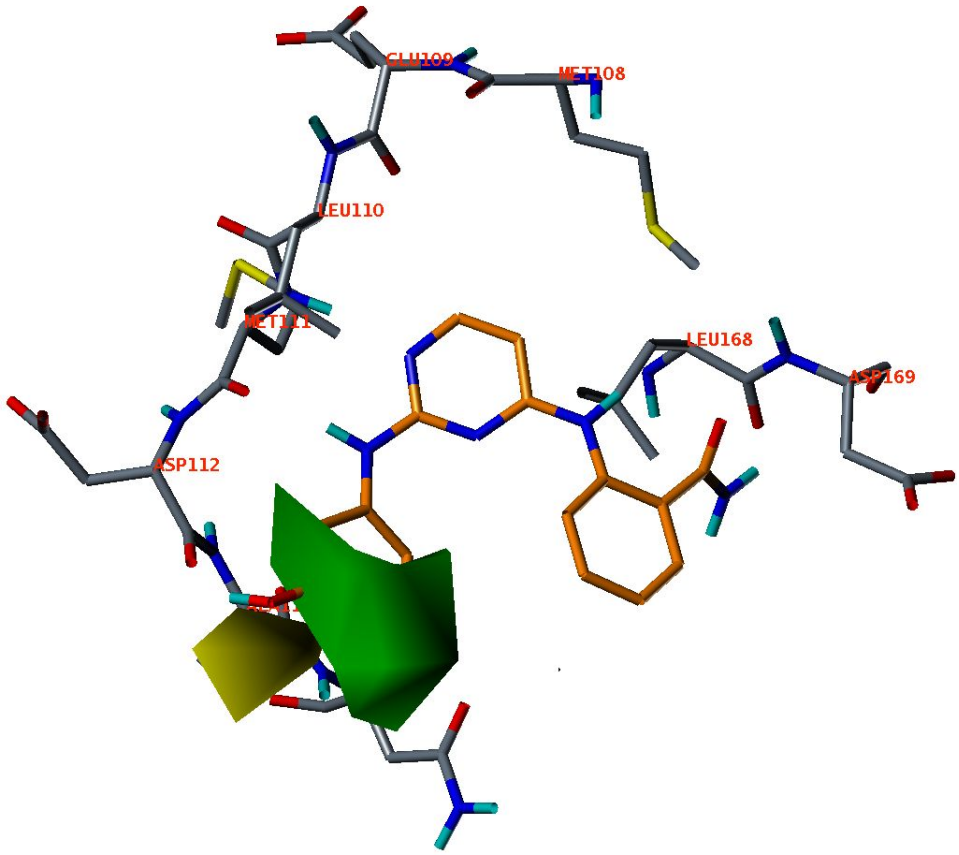

Figure 5: The CoMSIA steric contour map with compound 02 (Table 1). Green contours indicate regions where bulky groups increase activity, whereas yellow contours indicate regions where bulky groups decrease activity.

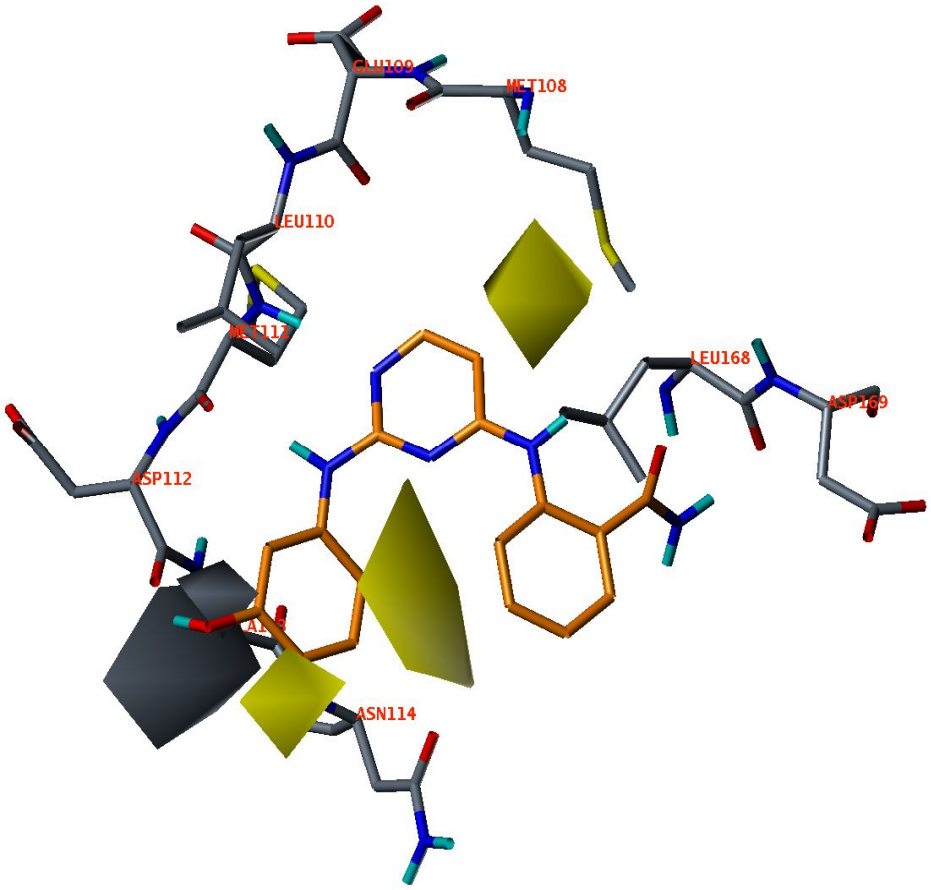

Figure 6: The CoMSIA hydrophobic contour map with compound 02 (Table 1). Yellow contours indicate the regions where hydrophobic groups increase activity, whereas white contours indicate the regions where hydrophobic groups decrease activity.

The yellow and white contour map indicates the regions where hydrophobic and hydrophilic groups are preferred, respectively. The white contour was observed near the meta position of the phenyl ring, which indicates that the hydrophilic groups can interact with the carbonyl group of Asp112. This is a possible reason why compounds 14, 15, and 16 with the hydrophilic substitution show higher potency. There were two yellow contours observed. One was near the para position of the phenyl ring. This explains why the substitution of the hydrophobic groups could interact with Ala113 to improve the potency of compounds. Another yellow contour was observed near the 5' position of the pyrimidine ring. This indicates that hydrophobic substitution was favorable at this position and it may access the hydrophobic residue of Met108 (also known as gatekeeper). The contour map results indicate that substitution of the hydrophobic groups at the 5' position could potentially identify additional interaction between the pyrimidine ring and the important gatekeeper residue. This interaction might improve the activity of newly synthesized analogs.

Figure 7 represents the H-bond acceptor contour map with the compound 02. The magenta region indicates where the hydrogen bond acceptor group increases the activity and the red contour map indicates where the hydrogen bond acceptor group decreases the activity. The unfavorable red contour map was found near the amino group of the benzamide ring, meaning that H-bond donating groups favorably interact with the negatively charged Asp169. The H-bond acceptor contour map showed reasonable modification in the benzamide ring. This could be the reason why compound 02 shows higher biological activity than other compounds.

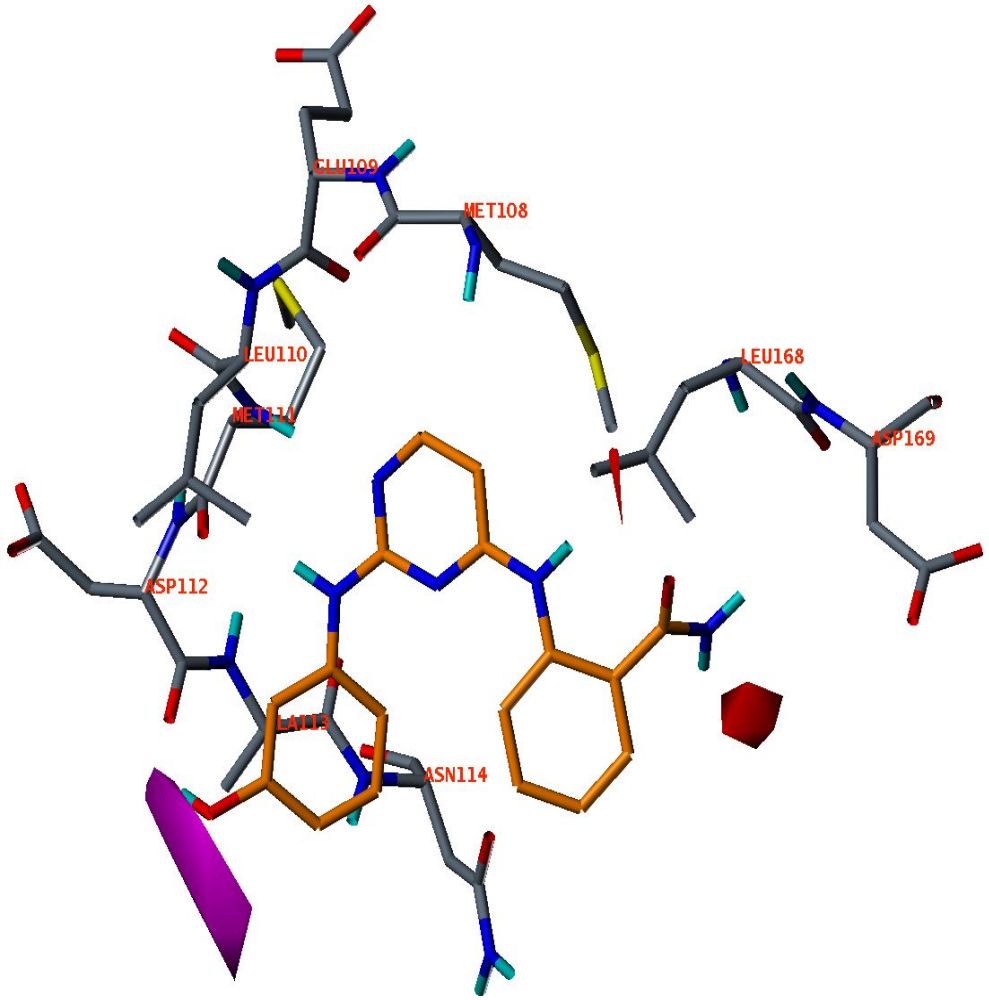

Figure 7: The CoMSIA H-bond acceptor contour map with compound 02 (Table 1). Magenta colour indicates the regions where hydrogen bond acceptor substituents enhance activity; red colour indicates the regions where hydrogen bond acceptor substituents reduce activity.

In summary, both CoMFA and CoMSIA contour maps identified some crucial modifications for 4-anilinopyrimidines derivatives. The CoMFA map recognized that substitution of electropositive groups in the phenyl ring could possibly interact with Asp112, Ala113 and Asp114. CoMSIA provided additional information over CoMFA, in terms of both hydrogen bonding and hydrophobic interactions with the active site residues. The CoMSIA H-bond acceptor contour map found that further modification is required for the benzamide ring to interact with the negatively charged Asp169. Furthermore, the CoMSIA contour map explained the importance of the hydrophobic substitution in the 5' position of the pyrimidine ring. Modification in this position seems remarkably important to produce more potent and selective JNK1 inhibitors.

3.6. Analysis of the molecular dynamics

We compared the 3D-QSAR model with the molecular dynamics simulation for the protein-ligand complex. Since the QSAR model was mainly focused on the structural enhancement of the inhibitors, it was better to evaluate the model with the molecular simulation binding mode of the receptor site. 2ns-MD simulation was carried out for the highly active compound in the series (i.e. compound 02), along with the JNK1 crystal structure. To examine the variation in the intramolecular conformations of JNK1, the root mean square deviation (RMSD) with respect to the initial structure was calculated. Simulation time versus the RMSD of the protein backbone atom and inhibitor were presented in Figures 8 and 9, respectively.

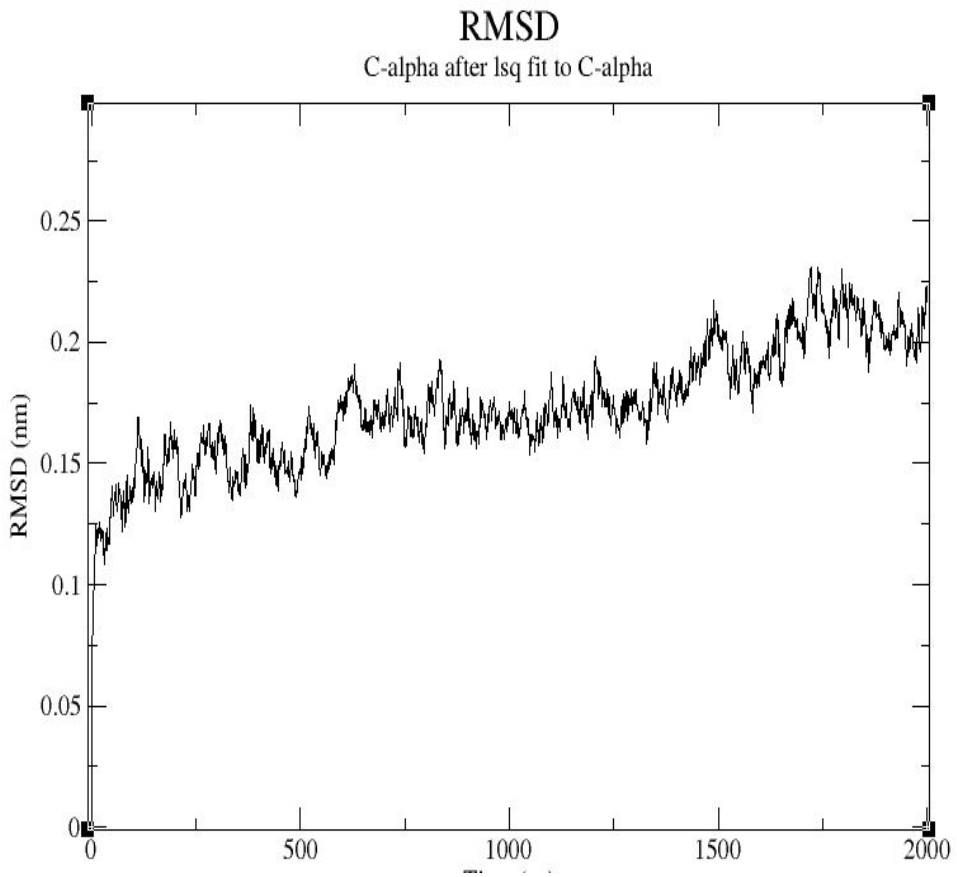

Figure 8: Simulation time versus RMSD for the JNK1 protein backbone.

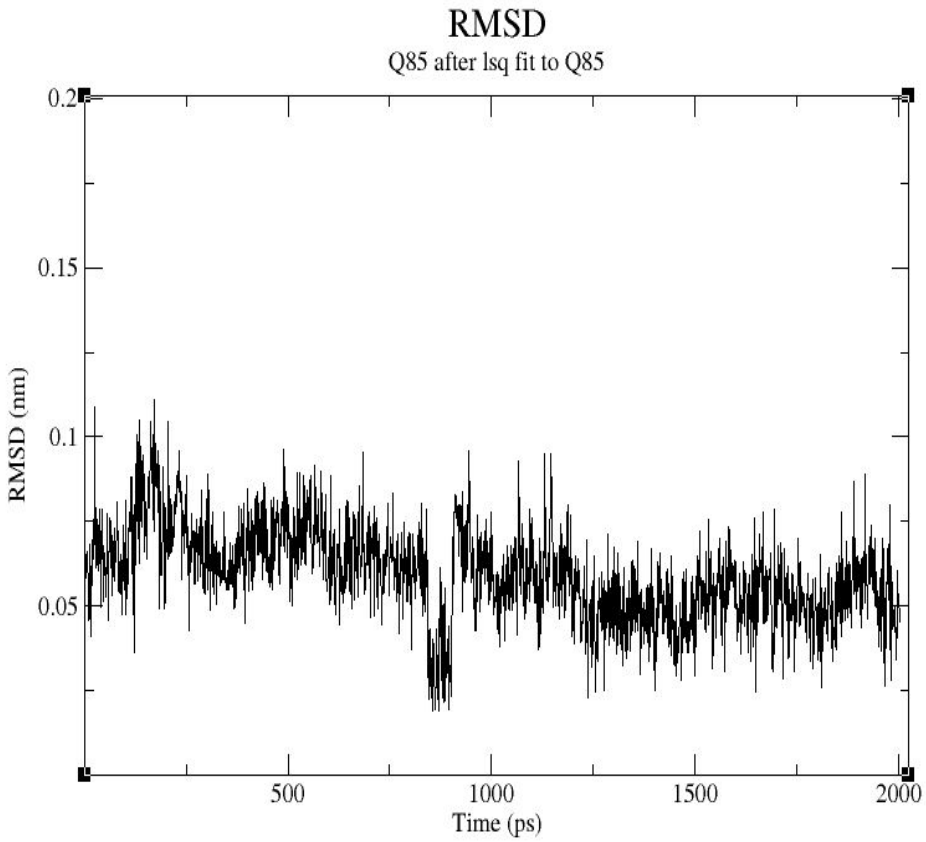

Figure 9: Simulation time versus RMSD for compound 02.

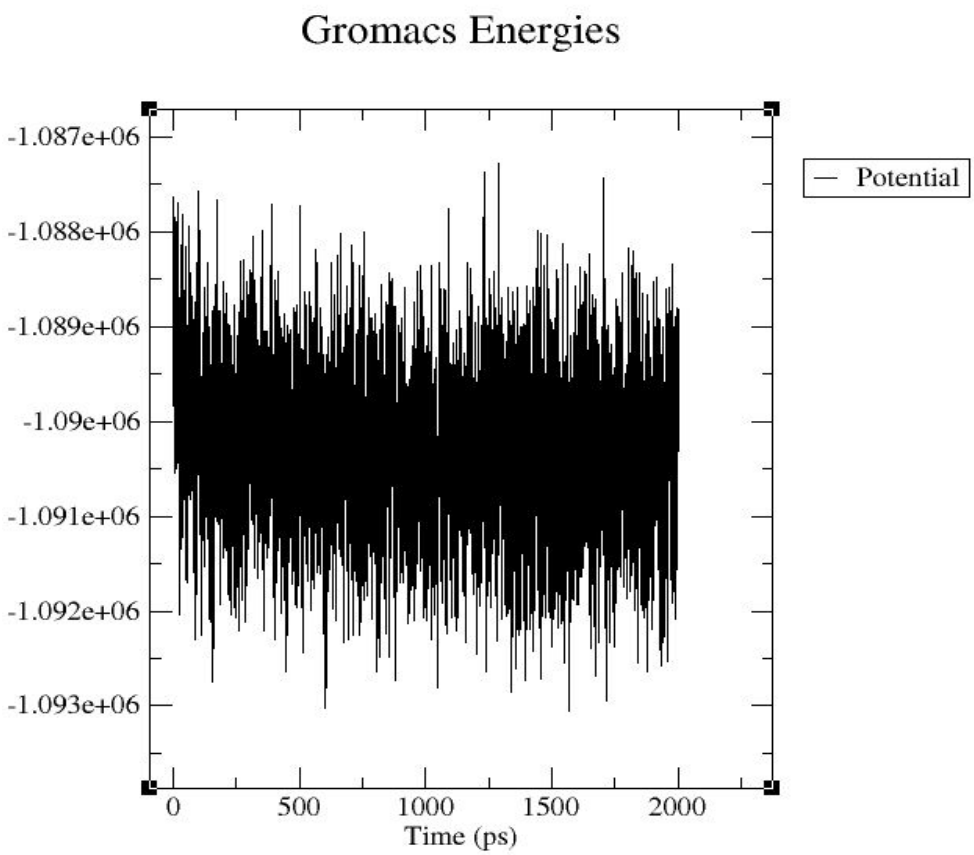

Figure 10: Potential energy graph for the JNK1 complex (PDB code: 2NO3).

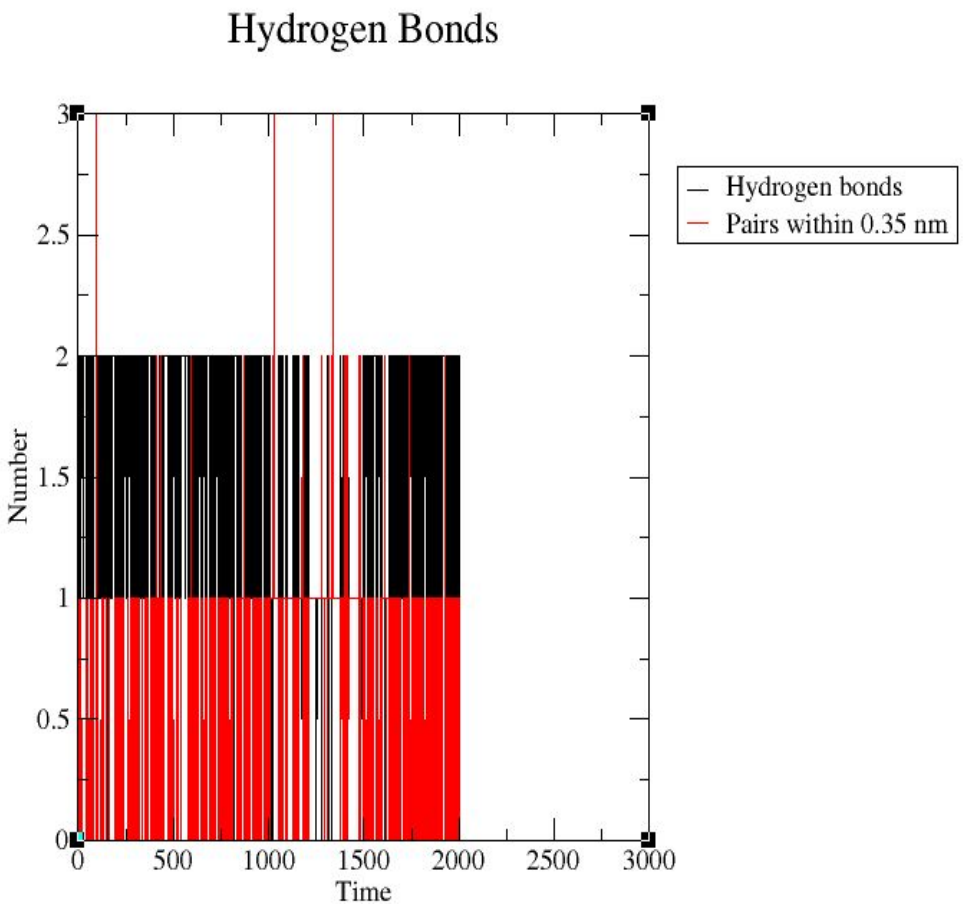

Figure 11: Simulation time versus the number of hydrogen bonds for compound 02 with Met111 residue.

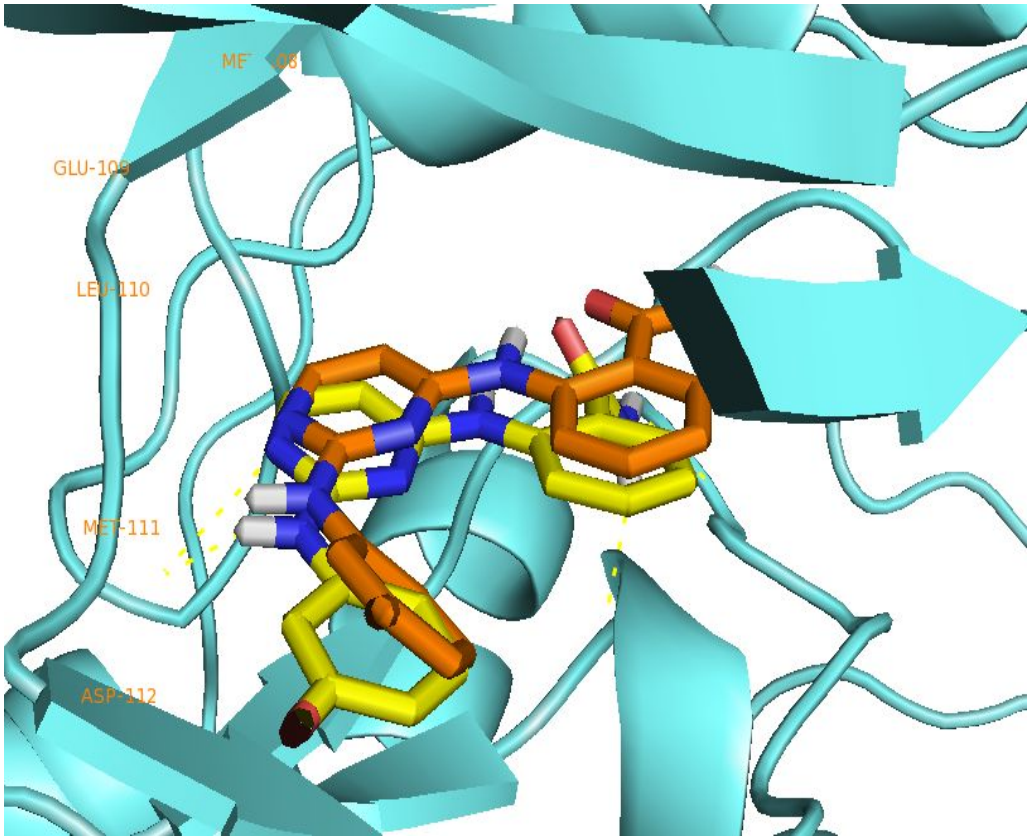

Figure 12: Alignment of the 3D-QSAR model (Orange) with the MD model (Yellow), inside the JNK1 active site.

The results showed that the system becomes equilibrated at 600 ps, and the lowest energy conformation was judged by their potential energy graph (Figure 10). Figure 8 shows the root-mean-square deviation (rmsd) of the trajectory for the protein backbone with respect to the initial structure (in black line), and the graph presents that the rmsd reaches about 0.15 Å, which suggests that a relatively stable conformation of the protein is achieved through the MD simulation. Figure 9 also gives the rmsd of the compound 2 (in red line) in the binding site of JNK1. It can be clearly noted that the rmsd for the ligand reaches about 0.08 Å from the beginning of MD simulation and retains this value throughout the simulation, suggesting that the changes of complex are mainly caused by the protein. Figure 11 represents the hydrogen bond interaction with the active site residue of Met111. Throughout the MD simulation, there was a hydrogen bond interaction between compound 02 and the hinge residue Met 111. This suggests that it has two stable hydrogen bond interactions, which is consistent with the experimental observation. The superimposition of both models is presented in Figure 12 and the MD model has shown similar hydrogen bonding interaction with the Met111 (i.e. the hinge region). Both models were aligned and correlated well with each other, indicating that the low energy conformation of compound 02 has similar orientation with the binding mode used for generation of the 3D-QSAR model. Although the complex has undergone several movements during MD simulation, both the binding pocket and the conformation of the compound 2 are still stable, suggesting rationality and validity of the 3D-QSAR model. From these results, we concluded that the generated 3D-QSAR model was good enough to design new JNK1 analogs.

3.7. 3D Pharmacophore search and docking

We used the 3D crystal structure of JNK1 in complex with the potent inhibitor 2-({2-[(3-hydroxyphenyl)amino]pyrimidin-4-yl}amino) benzamide (PDB code: 2NO3) to generate the pharmacophore hypothesis. By using the spatial and partial match constraint, we defined the 3D-pharmacophore query on the basis of the crystal structure bound conformation. The receptor donor and acceptor sites of Met111 are crucial (hinge) for the hydrogen bond interaction with JNK1 inhibitors, and thecontour map helped to identify another important amino acid, which was also used as pharmacophore query.

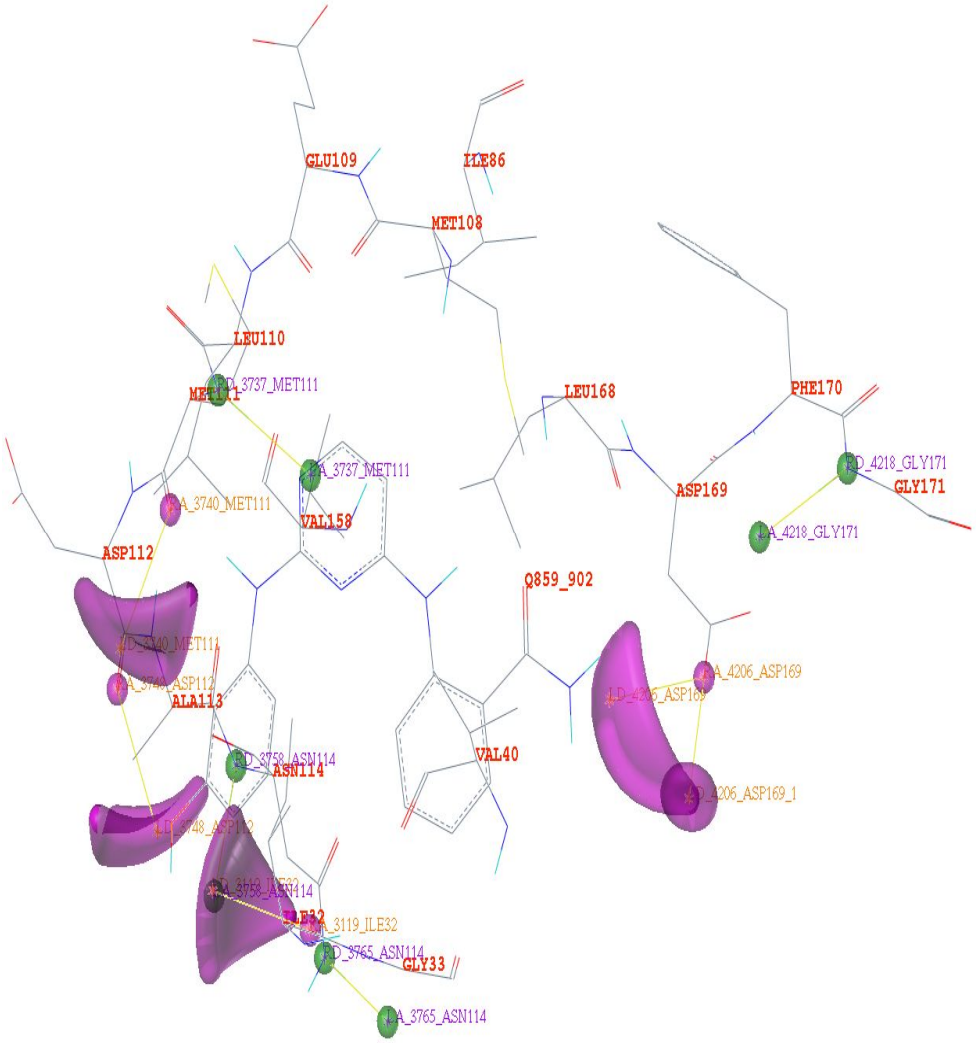

Figure 13: Using partial match constraints, the 3D pharmacophore query was generated for the JNK1 complex structure. The green coloured ball indicates query for the receptor donor site and the magenta coloured ball indicates the query for the receptor acceptor site.

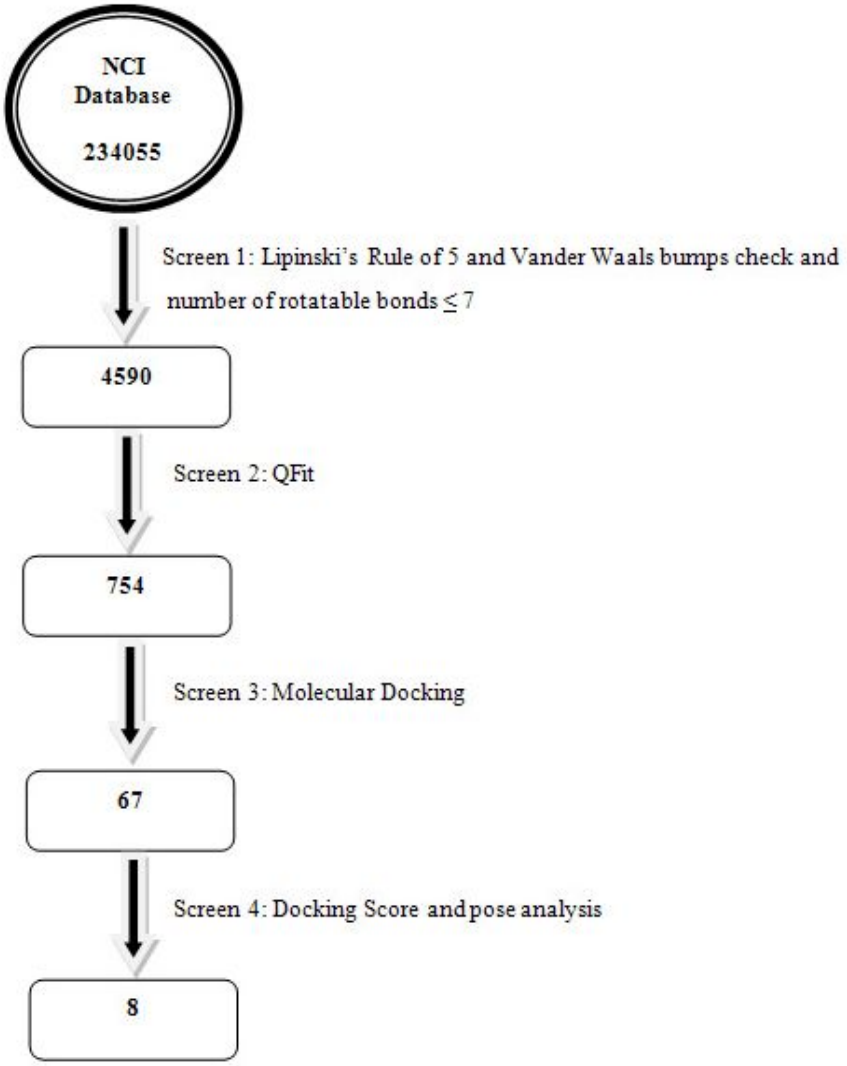

Figure 14: Results from the virtual screening of the NCI database. The number shows the total number of molecules obtained after applying the filtration criteria.

Figure 13 represents the 3D-pharmacophore query generated from the crystal structure. Virtual screening was performed using this 3D pharmacophore query against the NCI database. The screening was carried out by few filtration criteria, such as the Lipinski's Rule of five, the Vander Waals bumps and by restricting the number of rotatable bonds to a maximum of 7. The flow chart for virtual screening of various filtration criteria is presented in Figure 14. To reduce the number of molecules for further analysis, first we applied the Lipinski's rule of 5, the Vander Waals bumps and we restricted the number of rotatable bonds to $\geq$ 7. This generated 4590 hits from the NCI database. Further refinement of these hits was carried out using the QFit, According to this rule, the best mapping (i.e., the map with the highest QFit) is returned as the hit. Using this option, we further eliminated molecules from this filtration criterion. The 754 hits obtained were then subjected to docking into the active site of JNK1, using the Surflex molecular docking method. To verify the reproducibility of the docking calculations, the bound conformation of compound 02 (i.e. the reference compound) (PDB code: 2NO3) was redocked with the JNK1 active site. The Surflex docking method reproduced the same binding mode with the docking score of 5.75 and the RMSD value of 0.993. After visual inspection of each compound, we identified eight compounds as new potential leads for JNK1. All the potential lead compounds showed hydrogen bonding interaction with Met 111 (i.e. the hinge region) and additional hydrogen bond interaction with other active site residues (i.e. Glu109, Asp112, Asn114, and Asp169).

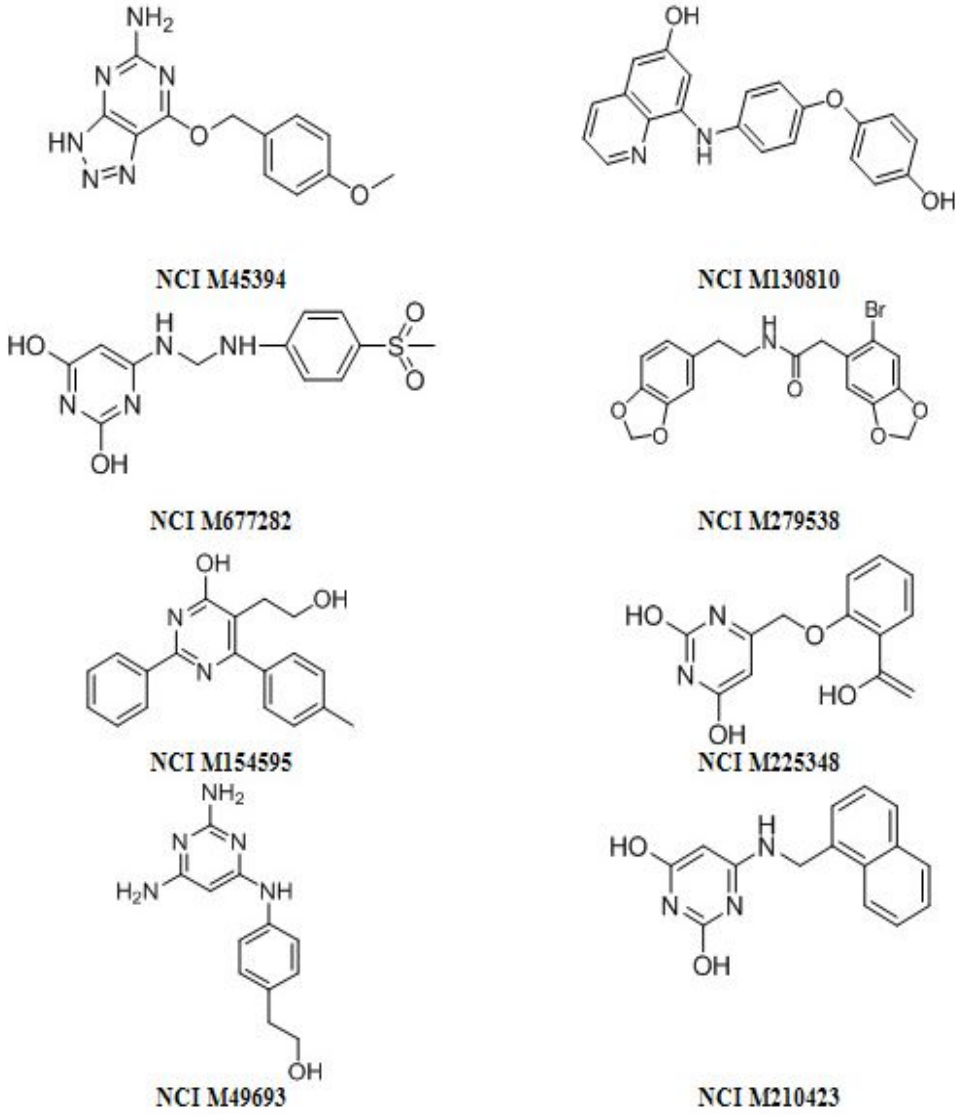

Figure 15: Chemical structures of the identified hits.

Table 9: Docking scores, as well as predicted activities, from both CoMFA and CoMSIA models, for the eight identified hits.

Hit	Docking Score	H-bond Interaction with Active site residue	Predicted pIC_{50}	
			CoMFA	CoMSIA
NCI M45394	8.27	Met111, Glu109	6.113	6.926
NCI M130810	8.21	Met 111, Asp169	6.470	6.821
NCI M677282	8.82	Met111, Glu109	6.150	6.516
NCI M279538	7.09	Met111, Asn114	6.632	6.307
NCI M154595	6.75	Met111, Glu109	7.167	7.360
NCI M225348	6.74	Met111, Glu109, Asp112	7.101	8.376
NCI M49693	6.67	Met111, Glu109, Asp169	6.406	6.527
NCI M210423	6.41	Met111, Glu109	6.397	6.700

Moreover, the activities of the identified hits were further predicted by the generated CoMFA and CoMSIA models. Figure 15 showed the eight potential lead compounds with high Surflex docking scores. The docking scores, as well as the predicted bioactivities of pIC_{50} from both CoMFA and CoMSIA models (i.e. the receptor-guided method), are shown in Table 9.

3.8. Binding mode analysis of identified hits

Elucidation of ligand binding mechanisms is an extremely important step to obtain more potent and selective lead molecules for JNK1 enzyme. Therefore, we investigated a detailed binding interaction of a few potent hit compounds using Surflex docking method. After docking, the individual binding poses of each potent hit were observed and their interactions with the protein were studied. The best and the most energetically favorable conformation of potent hits were selected. The identified hits showed all the necessary interactions which are important for effective JNK1 inhibition. The detailed binding interactions of some of the hits (**NCI M45394, NCI NCI M225348**, and **NCI M49693**) are given in the following sections.

3.8.1. Binding mode of NCI M45394, NCI M225348, and NCI M49693

Figure 16 represents the binding mode of NCI M45394 and it showed four hydrogen bond interactions within the active site of JNK1 enzyme. Their hydrogen bond donor and acceptor features interact with Glu109, and Met111. As illustrated in the binding mode, one of the NH_2 substituents of the pyrimidine ring forms an H-bond with backbone carbonyl group of Glu109 with a bond length value of 2.745 Å. Similarly another nitrogen and NH_2 substituent interact with hinge residue Met111. The corresponding bond lengths are 1.867 Å and 2.262 Å.

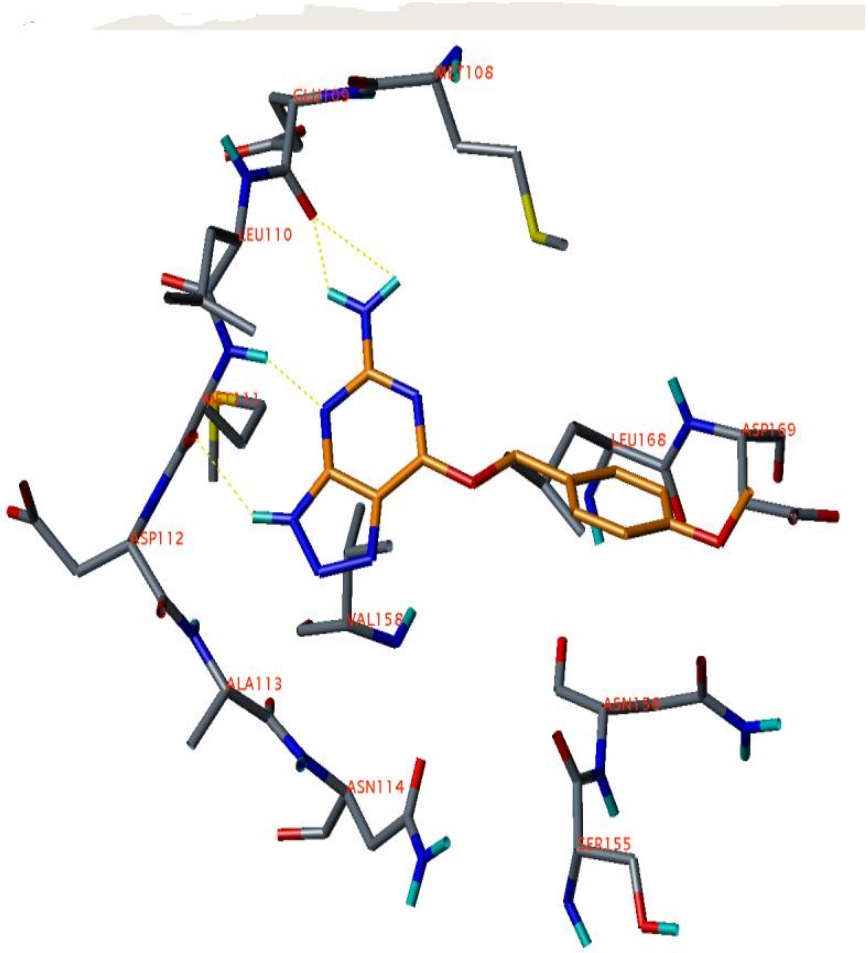

Figure 16: Stereoview of Surflex predicted binding poses of NCI M45394, in the active site of the JNK1 enzyme.

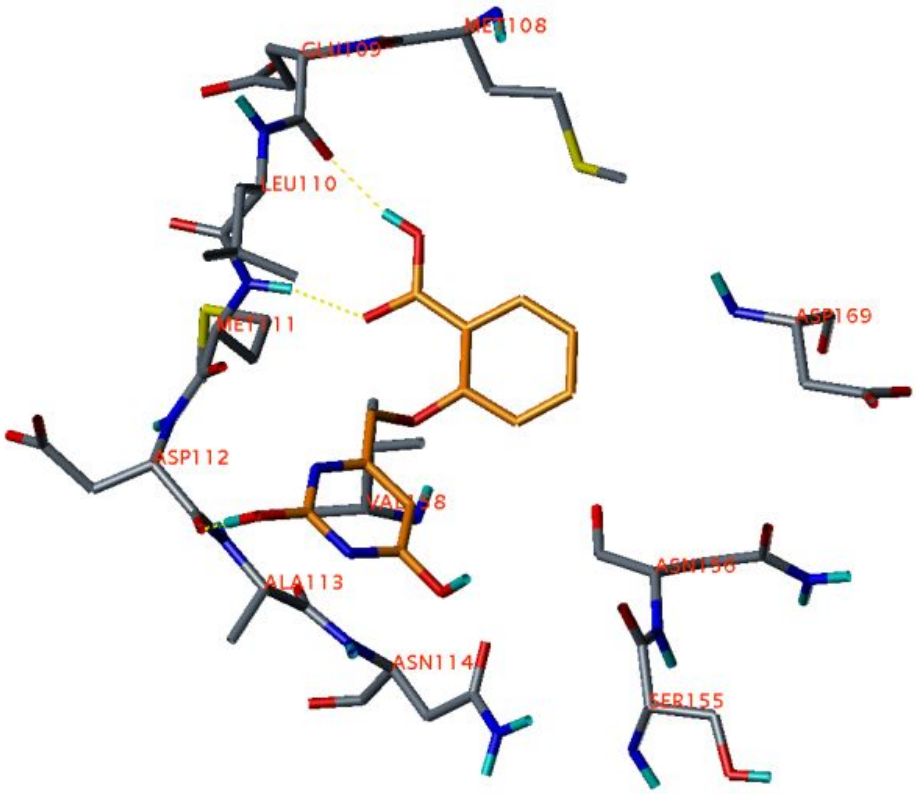

Figure 17: Stereoview of Surflex predicted binding poses of NCI M225348, in the active site of the JNK1 enzyme.

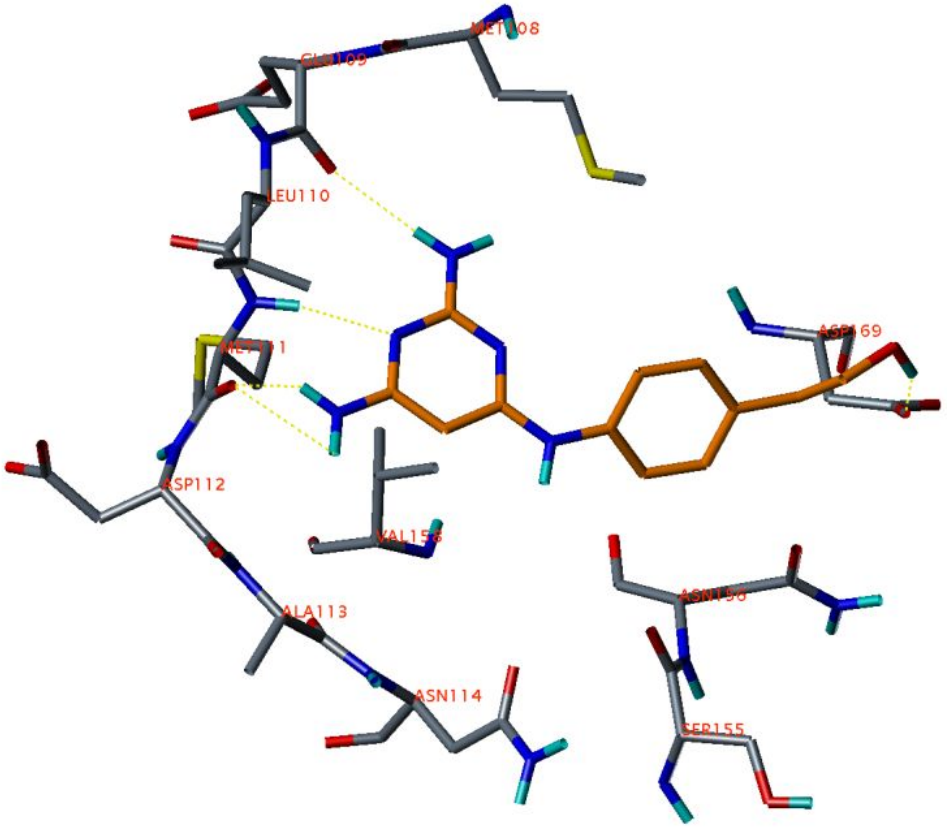

Figure 18: Stereoview of Surflex predicted binding poses of NCI M49693, in the active site of the JNK1 enzyme.

Figure 17 shows the binding mode of NCI M225348, it makes H-bond contacts with hinge region residues (Glu109, Met111,) additionally, the OH substituent of

pyrimidine ring forms H-bond with Asp112. The docking scores of the identified hits are comparatively greater than that of the reference compound. The better binding scores of the selected hits are due to the additional stabilizing interactions. For example, NCI M225348 shows interactions with Asp112 in addition to the core interactions.

The binding mode of NCI M49693 within the active site residues of JNK1 enzyme is given in Figure 18. It interacts with Glu109, Met111, and Asp169 and forms five H-bond contact with these active site residues. As illustrated in the binding mode, one of the NH_2 substituents of the pyrimidine ring forms an H-bond with backbone carbonyl group of Glu109 with a bond length value of 2.331 Å. Similarly another nitrogen and NH_2 substituent interact with hinge residue Met111. The corresponding bond lengths are 1.569 Å and 2.688 Å. Additionally, the OH substituent of phenyl ring forms H-bond with Asp169 with a bond length value of 1.872 Å. The identified hits are expected to have critical pharmacophore features and it can be a new potential leads for JNK1.

4. Conclusion

Comparative CoMFA and CoMSIA models were developed for the series of JNK1 inhibitors. In this work, we applied various alignment methods to generate a reasonable 3D-QSAR model. The receptor-guided alignment method produced better models than the ligand based approach, because this alignment is directly associated with the receptor information, which is more realistic than in other techniques. The superposition of both CoMFA and CoMSIA contour maps within the receptor showed reasonable correspondence between the contour map property and the surrounding amino acid property of the active site region. This provides more detailed information about the interaction between the series of compounds and the JNK1 inhibitors. Our 3D-QSAR models identified some crucial modifications for 4-anilinopyrimidines derivatives. The CoMFA map recognized that substitution of electropositive groups in the phenyl ring could possibly interact with Asp112, Ala113 and Asp114. The CoMSIA H-bond acceptor contour map found that further modification is required for the benzamide ring to interact with the negatively charged Asp169. Furthermore, the CoMSIA contour map explained the importance of the hydrophobic substitution in the 5' position of the pyrimidine ring. Modification in this position seems remarkably important to produce more potent and selective JNK1 inhibitors. Furthermore, the MD simulation study concluded that two stable hydrogen bonds exist from the initial few picoseconds simulation time with the hinge residue (Met111). The superposition of binding modes correlated well with each other and showed that the compound 02 has similar orientation with the generated QSAR model. Finally, we have performed virtual screening, using the bound conformation from the JNK1 complex structure and

identified 8 compounds as new potential leads for JNK1, by using various filtration criteria. Results of this study might be useful for future drug design studies and we hope that it would be the starting point for the synthesis of more potent and selective JNK1 inhibitors.

5. References

[1] Barr, R.K. and Bogoyevitch, M.A., The c-Jun N-terminal protein kinase family of mitogen-activated protein kinases (JNK MAPKs), Int. J. Biochem. Cell. Biol., 33 (2001)1047–1063.

[2] Bogoyevitch, M.A. and Kobe, B., Uses for JNK: the many and varied substrates of the c-Jun N-terminal kinases, Microbiol. Mol. Biol. Rev., 70, (2006) 1061–1095.

[3] Bogoyevitch, M.A., The isoform-specific functions of the c- Jun N-terminal kinases (JNKs): differences revealed by gene targeting, Bioessays., 28 (2006) 923–934.

[4] Gupta, S., Barrett, T., Whitmarsh, A.J., Cavanagh, J., Sluss, H.K., Rijard, B.-D. and Davis, R.J., Selective interaction of JNK protein kinase isoforms with transcription factors., EMBO J., 15, (1996) 2760–2770.

[5] Mohit, A.A., Martin, J.H. and Miller, C.A., p493F12 kinase: a novel MAP kinase expressed in a subset of neurons in the human nervous system., Neuron., 14 (1995) 67–78.

[6] Wild, S., Roglic, G., Green, A., Sicree, R. and King, H., Global prevalence of diabetes: estimates for the year 2000 and projections for 2030., Diabetes Care., 27 (2004) 1047–1053.

[7] Aguirre, V., Uchida, T., Yenush, L., Davis, R. and White, M.F., The c-Jun NH(2)-terminal kinase promotes insulin resistance during association with insulin receptor substrate-1 and phosphorylation of Ser(307), J. Biol. Chem., 275 (2000) 9047–9054.

[8] Hirosumi, J., Tuncman, G., Chang, L., Gorgun, C. Z., Uysal, K.T., Maeda, K., Karin, M. and Hotamisligil, G.S., A central role for JNK in obesity and insulin resistance, Nature, 420 (2002), 333–336.

[9] Bennett, B.L., Satoh, Y. and Lewis, A.J., JNK: a new therapeutic target for diabetes, Curr. Opin. Pharmacol., 3 (2003), 420–425.

[10] Wellen, K.E. and Hotamisligil, G.S., Inflammation, stress, and diabetes, J. Clin. Invest., 115 (2005) 1111–1115.

[11] Waeber, G., Delplanque, J., Bonny, C., Mooser, V., Steinmann, M., Widmann, C., Maillard, A., Miklossy, J., Dina, C., Hani, E. H., Vionnet, N., Nicod, P., Boutin, P. and Froguel, P., The gene MAPK8IP1, encoding islet-brain-1, is a candidate for type 2 diabetes, Nat. Genet., 24 (2000) 291–295.

[12] Rckle, T., Biamonte, M., Grippi-Valloton, T., Arkinstall, S., Cambet, Y., Camps, M., Chabert, C., Church, D. J., Halazy, S., Jiang, X., Martinou, I., Nichols, A., Sauer, W. and Gotteland, J.P., Design, synthesis, and biological activity of novel, potent, and selective (benzoylaminomethyl) thiophene sulfonamide inhibitors of c-Jun-N-terminal kinase, J. Med. Chem., 47 (2004) 6921–6934.

[13] Gaillard, P., Jeanclaude-Etter, I., Ardissone, V., Arkinstall, S., Cambet, Y., Camps, M., Chabert, C., Church, D., Cirillo, R., Gretener, D., Halazy, S., Nichols, A., Szyndralewiez, C., Vitte, P.A. and Gotteland, J.P., Design and synthesis of the first generation of novel potent, selective, and in vivo active

(benzothiazol-2-yl)acetonitrile inhibitors of the c-Jun N-terminal kinase, J. Med. Chem., 48 (2005), 4596–4607.

[14] Stocks, M. J., Barber, S., Ford, R., Leroux, F., St-Gallay, S., Teague, S. and Xue, Y., Structure-driven HtL: design and synthesis of novel aminoindazole inhibitors of c-Jun N-terminal kinase activity, Bioorg. Med. Chem. Lett., 15 (2005) 3459–3462.

[15] Szczepankiewicz, B.G., Kosogof, C., Nelson, L.T.J., Liu, G., Liu, B., Zhao, H., Serby, M.D., Xin, Z., Liu, M., Gum, R.J., Haasch, D.L., Stashko, M.A., Olejniczak, E.T., Sun, C., Dorwin, S.A., Haskins, K., Abad-Zapatero, C., Fry, E.H., Hutchins, C.W., Sham, H.L., Rondinone, C.M. and Trevillyan, J.M., Aminopyridine-based c-Jun N-terminal kinase inhibitors with cellular activity and minimal cross-kinase activity, J. Med. Chem., 49 (2006) 3563–3580.

[16] Liu, M., Xin, Z., Clampit, J.E., Wang, S., Gum, R.J., Haasch, D.L., Trevillyan, J.M., Abad-Zapatero, C., Fry, E.H., Sham, H.L. and Liu, G., Synthesis and SAR of 1,9-dihydro-9-hydroxypyrazolo[3,4-b]quinolin-4-ones as novel, selective c-Jun N-terminal kinase inhibitors, Bioorg. Med. Chem. Lett., 16 (2006) 2590–2594.

[17] Liu, G., Zhao, H., Liu, B., Xin, Z., Liu, M., Kosogof, C. Szczepankiewicz, B.G., Wang, S., Clampit, J.E., Gum, R.J., Haasch, D.L., Trevillyan, J.M. and Sham, H.L., Aminopyridine carboxamides as c-Jun N-terminal kinase inhibitors: targeting the gatekeeper residue and beyond, Bioorg. Chem. Lett., 16 (2006) 5723–5730.

[18] Liu, M., Wang, S., Clampit, J.E., Gum, R.J., Haasch, D.L., Rondinone, C.M., Trevillyan, J.M., Abad-Zapatero, C., Fry, E.H., Sham, H.L. and Liu, G., Discovery of a new class of 4-anilinopyrimidines as potent c-Jun N-terminal kinase inhibitors: Synthesis and SAR studies, Bioorg. Med. Chem. Lett., 17 (2007), 668–672.

[19] Liu, G. and Rondinone, C.M., JNK: bridging the insulin signaling and inflammatory pathway, Curr. Opin. Investig. Drugs., 6 (2005) 979–987.

[20] Alam, M., Beevers, R.E., Ceska, T., Davenport, R.J., Dickson, K.M., Fortunato, M., Gowers, L., Haughan, A.F., James, L.A., Jones, M.W., Kinsella, N., Lowe, C., Meissner, J.W.G., Nicolas, A.L., Perry, B.G., Phillips, D.J., Pitt, W.R., Platt, A., Ratcliffe, A.J., Sharpe, A. and Tait, L.J., Synthesis and SAR of aminopyrimidines as novel c-Jun N-terminal kinase (JNK) inhibitors, Bioorg. Med. Chem. Lett., 17 (2007) 3463–3467.

[21] Jiang, R., Duckett, D., Chen, W., Habel, W., Habel, J., Ling, Y.Y., LoGrasso, P. and Kamenecka, T.M., 3,5-Disubstituted quinolines as novel c-Jun N-terminal kinase inhibitors, Bioorg. Med. Chem. Lett., 17 (2007) 6378– 6382.

[22] Bennett, B.L., Sasaki, D.T., Murray, B.W., O'Leary, E.C., Sakata, S.T., Xu, W., Leisten, J.C., Motiwala, A., Pierce, S., Satoh, Y., Bhagwat, S.S., Manning, A.M. and Anderson, D.W., SP600125, an anthrapyrazolone anthrapyrazolone inhibitor of Jun N-terminal kinase, Proc. Natl. Acad. Sci. USA., 98 (2001) 13681–13686.

[23] Zhao, H., Serby, M.D., Xin, Z., Szczepankiewicz, B.G., Liu, M., Kosogof, C. and Liu, B., Discovery of potent, highly selective, and orally bioavailable pyridine carboxamide c-Jun NH2-terminal kinase inhibitors, J. Med. Chem., 49 (2006) 4455–4458.

[24] Swahn, B.M., Xue, Y., Arzel, E., Kallin, E., Magnus, A., Plobeck, N. and Viklund, J., Design and synthesis of 2'-anilino-4,4'-bipyridines as selective inhibitors of c-Jun N-terminal kinase-3, Bioorg. Med. Chem. Lett., 16 (2006) 1397–13401.

[25] Kamenecka, T., Habel, J., Duckett, D., Chen, W., Ling, Y.Y., Frackowiak, B., Jiang, R., Shin, Y., Song, X. and LoGrasso, P., Structure-activity relationships and X-ray structures describing the selectivity of aminopyrazole inhibitors for c-Jun N-terminal kinase 3 (JNK3) over p38, J. Biol. Chem., 284 (2009) 12853–12861.

[26] LoGrasso, P. and Kamenecka, T., Inhibitors of c-jun-N-terminal kinase (JNK), Mini-Rev. Med. Chem., 8 (2008) 755–766.

[27] Kamenecka, T., Jiang, R., Song, X., Duckett, D., Chen, W., Ling, Y.Y., Habel, J., Laughlin, J.D., Chambers, J., Figuera-Losada, M., Cameron, M.D., Lin, L., Ruiz, C.H. and LoGrasso, P.V., Synthesis, biological evaluation, X-ray structure, and pharmacokinetics of aminopyrimidine c-jun-N-terminal kinase (JNK) inhibitors, J. Med. Chem., 53 (2010) 419–431.

[28] Liu, M., Wang, S., Clampit, J.E., Gum, R.J., Haasch, D.L., Rondinone,C.M., Trevillyan, J.M., Zapatero, C.A., Fry, E.H., Sham, H.L. and Liu, G., Discovery

of a new class of 4-anilinopyrimidines as potent c-Jun N-terminal kinase inhibitors: synthesis and SAR studies, Bioorg. Med. Chem. Lett., 17 (2007) 668–672.

[29] Siddiqui, J.M.A. and Reddy, P.A., Small Molecule JNK (c-Jun N-Terminal Kinase) Inhibitors, J. Med. Chem., 53 (2010) 3005–3012.

[30] Cramer, R.D., Patterson, D.E. and Bunce, J.D., Comparative molecular field analysis (CoMFA). 1. Effect of shape on binding of steroids to carrier proteins, J. Am. Chem. Soc., 110 (1988) 5959–5967.

[31] Klebe, G., Abraham, U. and Mietzner, T., Molecular similarity indices in a comparative analysis (CoMSIA) of drug molecules to correlate and predict their biological activity, J. Med. Chem., 37 (1994) 4130–4146.

[32] Martin, Y.C., 3D QSAR: Current state, scope, and limitations, Perspect. Drug. Discovery. Des., 12 (1998) 3–23.

[33] Pasha, F.A,, Srivastava, H.K. and Singh, P.P., QSAR study of estrogens with the help of PM3-based descriptors, Int. J. Quantum. Chem., 104 (2005) 87–100.

[34] Pasha, F.A., Muddassar, M., Chung, H.W., Cho, S.J. and Cho, H., Hologram and 3D-quantitative structure toxicity relationship studies of azo dyes, J. Mol. Model., 14 (2008) 293–302.

[35] Pasha, F.A., Muddassar, M., Srivastava, A.K. and Cho, S.J., In silico QSAR studies of anilinoquinolines as EGFR inhibitors, J. Mol. Model., 16 (2010) 263–277.

[36] Singh, P.P., Srivastava, H.K. and Pasha, F.A., DFT-based QSAR study of testosterone and its derivatives, Bioorg. Med. Chem., 12 (2004) 171–177.

[37] Srivastava, H.K., Pasha, F.A. and Singh, P.P., Atomic softness based QSAR study of testosterone, Int. J. Quantum. Chem., 103 (2005) 237–245.

[38] Bohm, M., Sturzebecher, J. and Klebe, G., Three dimensional quantitative structure activity relationship analyses using comparative molecular field analysis and comparative molecular similarity indices analysis to elucidate selectivity differences of inhibitors binding to trypsin, thrombin, and factor Xa, J. Med. Chem., 42 (1999) 458–477.

[39] Abdulhameed, M.D.M., Hamza, A., Liu, J., Huang, X. and Zhan, C.G., Human microsomal prostaglandin E synthase-1 (mPGES-1) binding with inhibitors and the quantitative structure-activity correlation, J. Chem. Inf. Modeling., 48 (2008) 179–185.

[40] Kuo, C.L., Assefa, H., Kamath, S., Brzozowski, Z., Slawinski, J., Saczewski, F., Buolamwini, J.K. and Neamati, N., Application of CoMFA and CoMSIA 3D-QSAR and docking studies in optimization of mercapto benzene sulphonamides as HIV-1 integrase inhibitors, J. Med. Chem., 47 (2004) 385–399.

[41] Yang, G.F., Lu, H.T., Xiong, Y. and Zhan, C.G., Understanding the structure-activity and structure-selectivity correlation of cyclic guanine derivatives as phosphodiesterase-5 inhibitors by molecular docking, CoMFA and CoMSIA analyses, Bioorg. Med. Chem., 14 (2006) 1462–1473.

[42] Lipinski, C.A., Drug-like properties and the causes of poor solubility and poor permeability, J. Pharmacol. Toxicol. Methods., 44 (2000) 235–249.

[43] Sybyl 8.1 St. Louis, MO 63144, USA: Tripos Inc.

[44] Agarwal, A. and Taylor, E.W., 3-D QSAR for intrinsic activity of 5-HT1A receptor ligands by the method of comparative molecular field analysis, J. Comput. Chem., 14 (1993) 237–245.

[45] Akamatsu, M., Fujita, T., Ozoe, Y., Mochida, K., Nakamura, T. and Matsumura, F., 3D QSAR of insecticidal dioxatricycloalkene and its related compounds, In Wermuth, C.-G. (Ed.) Trends in QSAR and Molecular Modeling, Proceedings of the 9th European Symposium on Structure–Activity Relationships: QSAR and Molecular Modeling, ESCOM, Leiden, The Netherlands, 1993, pp. 525–526.

[46] Agarwal, A., Pearson, P.P., Taylor, E.W., Li, H.B., Dahlgren, T., Herslof, M., Yang, Y.H., Lambert, G., Nelson, D.L., Regan, J.W. and Martin, A.R., 3-dimensional quantitative structure–activity relationships of 5-HT receptor binding data for tetrahydropyridinylindole derivatives — a comparison of the Hansch and CoMFA methods, J. Med. Chem. 36 (1993) 4006–4014.

[47] Altomare, C., Carotti, A., Carta, V., Kneubuhler, S., Carrupt, P.A. and Testa, B., Modeling of newpyridazine inhibitors of MAO-B using QSAR and CoMFA approaches, In Sanz, F., Giraldo, J. and Manaut, F. (Eds.) QSAR and molecular modeling: Concepts, computational tools and biological applications, Proceedings of the 10th European Symposium on Structure–

Activity Relationships: QSAR and Molecular Modeling, Barcelona, Spain, September 4–9, 1994, J.R. Prous Science Publishers, Barcelona, 1995, pp. 463–465.

[48] Altomare, C., Campagna, F., Carta, V., Cellamare, S., Carotti, A., Genchi, G. and De Sarro, G., Synthesis, benzodiazepine receptor affinity and anticonvulsant activity of 5-H-indeno[1,2-c]pyridazine derivatives, 49 (1994) 313–323.

[49] Altomare, C., Cellamare, S., Carotti, A., Barreca, M.L., Chimirri, A., Monforte, A.M., Gasparrini, F., Villani, C., Cirrilli, M. and Mazza, F., Substituent effects on the enantioselective retention of anti-HIV 5-aryl-delta(2)-1,2,4-oxadiazolines on R,R-dach-DNB chiral stationary-phase, Chirality, 8 (1996) 556–566.

[50] Anzini, M., Cappelli, A., Vomero, S., Giorgi, G., Langer, T., Hamon, M., Merahi, N., Emerit, B.M., Cagnotto, A., Skorupska, M., Mennini, T. and Pinto, J.C., Novel, potent, and selective 5-HT3 receptor antagonists based on the arylpiperazine skeleton: Synthesis, structure, biological activity, and comparative molecular field analysis studies, J. Med. Chem., 38 (1995) 2692–2704.

[51] Artico, M., Botta, M., Corelli, F., Mai, A., Massa, S. and Ragno, R., Investigation on QSAR and binding mode of a new class of human rhinovirus-14 inhibitors by CoMFA and docking experiments, Bioorg. Med. Chem., 4 (1996) 1715–1724.

[52] Avery, M.A., Gao, F.G., Chong, W.K.M., Mehrotra, S. and Milhous, W.K., Structure–activity relationships of the antimalarial agent artemisinin: 1. Synthesis and comparative molecularfield analysis of C-9 analogs of artemisinin and 10-deoxoartemisinin, J. Med. Chem., 36 (1993) 4264–4275.

[53] Belvisi, L., Bravi, G., Catalano, G., Mabilia, M., Salimbeni, A. and Scolastico, C., A 3D QSAR CoMFA study of non-peptide angiotensin II receptor antagonists, J. Comput.-Aided Mol. Design, 10 (1996) 567–582.

[54] Botta, M., Cernia, E., Corelli, F., Manetti, F. and Soro, S., Probing the substrate specificity for lipases:A CoMFA approach for predicting the hydrolysis rates of 2-arylpropionic esters catalyzed by Candida rugosa lipase, Biochim. Biophys. Acta, 1296 (1996) 121–126.

[55] Brandt, W., Lehmann, T., Willkomm, C., Fittkau, S. and Barth, A., CoMFA investigations on two series of artificial peptide inhibitors of the serine protease thermitase, Int. J. Pep. Prot. Res., 46 (1995) 73–78.

[56] Brandt, W.L.T., Thondorf, I., Born, I., Schutkowski, M., Rahfield, J.-U.N.K. and Barth, A., A modelof the active site of dipeptidyl peptidase IV predicted by comparative molecular field analysis and molecular modeling simulations, Int. J. Pept. Protein Res., 46 (1995) 494–507.

[57] Brusniak, M.-Y.K., Pearlman, R.S., Neve, K.A. and Wilcox, R.E., Comparative molecular field analysis-based prediction of drug affinities at recombinant D1A dopamine receptors, J. Med. Chem., 39 (1996) 850–859.

[58] Brusniak, M.-Y.K., Pearlman, R.S., Neve, K.A. and Wilcox, R.E., Comparative molecular field analysis- based prediction of drug affinities at recombinant D1A dopamine receptors, J. Med. Chem., 39 (1996) 850–859.

[59] Bureau, R., Lancelot, J.C., Prunier, J. and Rault, S., Conformational analysis and 3D QSAR study on novel partial agonists of 5-HT3 receptors, Quant. Struct.-Act. Relat., 15 (1996) 373–381.

[60] Bureau, R., Rault, S. and Robba, M., Comparative molecular field analysis of CCK-B antagonists, Eur.J. Med. Chem., 29 (1994) 487–494.

[61] Bush, B.L. and Nachbar, Jr, R.B., Sample-distance partial least squares: PLS optimized for many variables, with application to CoMFA, J. Comput.-Aided Mol. Design, 7 (1993) 587–619.

[62] Calder, J.A., Wyatt, J.A., Frenkel, D.A. and Casida, J.E., CoMFA validation of the superposition of 6 classes of compounds which block GABA receptors noncompetitively, J. Comput.-Aid. Mol. Design, 7 (1993) 45–60.

[63] Caliendo, G., Fattorusso, C., Greco, G., Novellino, E., Perissutti, E. and Santagada, V. Shapedependent effects in a series of aromatic nitro compounds acting as mutagenic agents on T. typhimurium TA98, SAR QSAR Environ. Res., 4 (1995) 21–27.

[64] Caliendo, G., Greco, G., Novellino, E., Perissutti, E. and Santagada, V., Combined use of factorial design and comparative molecular field analysis (CoMFA): A case study, Quant. Struct.-Act. Relat., 13 (1994) 249–261.

[65] Carroll, F.I.M.., Lewin, A.H., Boja, J.W., and Kuhar, M.J., Pharmacophore development of (-)-cocaine analogs for the dopamine, serotonin, and norepinephrine uptake sites using a QSAR and CoMFA approach, In Wermuth, C.-G. (Ed.) Trends in QSAR and Molecular Modeling 92, Proceedings of the 9th European Symposium on Structure–Activity Relationships: QSAR and Molecular Modeling, ESCOM, Leiden, The Netherlands, 1993, pp. 530–531.

[66] Carroll, F.I., Mascarella, S.W., Kuzemko, M.A., Gao, Y., Abraham, P., Lewin, A.H., Boja, J.W. and Kuhar, M.J., Synthesis, Ligand Binding, and QSAR (ComFA and Classical) Study of 3.beta.-(3¢-Substituted phenyl)-,3.beta.-(4¢-Substituted phenyl)-, and 3.beta.-(3¢,4¢-Disubstituted phenyl)tropane- 2.beta.-carboxylic Acid Methyl Esters, J. Med. Chem., 37 (1994) 2865–2873.

[67] Cho, S.J., Garsia, M.L.S., Bier, J. and Tropsha, A. Structure-based alignment and comparative molecular field analysis of acetylcholinesterase inhibitors, J. Med. Chem., 39 (1996) 5064–5071.

[68] Cho, S.J., Tropsha, A., Suffness, M., Cheng, Y.-C. and Lee, K.-H., Antitumor agents: 163. Threedimensional quantitative structure–activity relationship study of 4'-O-demethylepipodophyllotoxin analogs using the CoMFA /q2-GRS approach, J. Med. Chem., 39 (1996) 1383–1395.

[69] Czaplinski, K.-H. and Grunewald, G.L., A comparative molecular field analysis derived model of the binding of taxol analogues to microtubules, Bioorg. Med. Chem., 4 (1994) 2211–2216.

[70] Czaplinski, K.-H., Haensel, W., Wiese, M. and Seydel, J.K., New benzylpyrimidines: Inhibition of DHFR from various species — QSAR, CoMFA and PC analysis, Eur. J. Med. Chem., 30 (1995) 779–787.

[71] Debnath, A.K., Hansch, C., Kim, K.H. and Martin, Y.C., Mechanistic interpretation of the genotoxicity of nitrofurans as antibacterial agents using quantitative structure–activity relationships (QSAR) and comparative molecular field analysis (CoMFA), J. Med. Chem., 36 (1993) 1007–1016.

[72] Debnath, A.K., Jiang, S., Strick, N., Lin, K., Haberfield, P. and Neurath, A.R., Three-dimensional structure–activity analysis of a series of porphyrin derivatives with anti-HIV-1 activity targeted to the V3 loop of the gp120 envelope glycoprotein of the human immunodeficiency virus type 1, J. Med. Chem., 37 (1994) 1099–1108.

[73] Dua, R.K., Taylor, E.W. and Phillips, R.S., A-aryl-L-cysteine S, S,-dioxides-design, synthesis,and evaluation of a new class of inhibitors of kynureninase, J. Am. Chem. Soc. 115 (1993) 1264–1270.

[74] Elass, A., Vergoten, G., Legrand, D., Mazurier, J., Elass-Rochard, E. and Spik, G., Processes underlying interactions of human lactoferrin with the jurkat human lymphoblastic T-cell line receptor, Quant. Struct.-Act. Relat., 15 (1996) 102–107.

[75] Faber, N.M., Griengl, H., Honig, H. and Zuegg, J., On the prediction of the enantioselectivity of Candida rugosa lipase by comparative molecular field analysis, Biocatalyst, 9 (1994) 227–239.

[76] Fabian, W.M.F., Timofei, S. and Kurunczi, L., Comparative molecular field analysis (CoMFA), semiempirical (AM1) molecular orbital and multi conformational minimal steric difference (MTD) calculations of anthraquinone dye-fiber affinities, Theochem, 340 (1995) 73–81.

[77] Gaillard, P.,Carrupt, P.-A., Testa, B. and Boudon, A., Molecular lipophilicity potential, a tool in 3D-QSAR: Method and applications, J. Comput.-Aid. Mol. Design, 8 (1994) 83–96.

[78] Gaillard, P., Carrupt, P.-A., Testa, B. and Schambel, P., Binding of arylpiperazines, (aryloxy) propanolamines, and tetrahydropyridylindoles to the 5-HT1A receptor: Contribution of the molecular lipophilicity potential to three-dimensional quantitative structure–affinity relationship models, J. Med. Chem., 39 (1996) 126–134.

[79] Gamper, A.M., Winger, R.H., Liedl, K.R., Sotriffer, C.A., Varga, J.M., Kroemer, R.T. and Rode, B.M., Comparative molecular field analysis of haptens docked to the multispecific antibody IgE(Lb4), J. Med. Chem., 39 (1996) 3882–3888; 40 (1997) 1047–1048.

[80] Gantchev, T.G., Ali, H. and van Lier, J.E., Quantitative structure–activity relationships/comparative molecular field analysis (QSAR/CoMFA) for receptor-binding properties of halogenated estradiol derivatives, J. Med. Chem, 37 (1994) 4164–4176.

[81] Glennon, R.A., Herndon, J.L. and Dukat, M., Epibatidine-aided studies toward definition of a nicotine receptor pharmacophore, Med. Chem. Res., 4 (1994) 461–473.

[82] Greco, G., Novellino, E., Fiorini, I., Nacci, V., Campiani, G., Ciani, S.M., Garofalo, A., Bernasconi, P. and Mennini, T., A comparative molecular field analysis model for 6-arylpyrrolo[2,1-d][1,5]benzothiazepines binding selectively to the mitochondrial benzodiazepine receptor, J. Med. Chem., 37 (1994) 4100–4108.

[83] Greco, G., Novellino, E., Pellecchia, M., Silipo, C. and Vittoria, A., Effects of variable sampling on CoMFA coefficient contour maps in a set of triazines inhibiting DHFR, J. Comput.-Aided Mol. Design, 8 (1994) 97–112.

[84] Hannongbua, S., Lawtrakul, L., Sotriffer, C.A. and Rode, B.M., Comparative molecular field analysis of HIV-1 reverse transcriptase inhibitors in the class of 1[2-hydroxyethoxy)-methyl]-6-(phenylthio)thymine, Quant. Struct.-Act. Relat., 15 (1996) 389–394.

[85] Hocart, S.J., Reddy, V., Murphy, W.A. and Copy, D.H., Three-dimensional quantitative structure– activity relationships of somatostatin analogs: 1. Comparative molecular field analysis of growth hormone release-inhibiting potencies, J. Med. Chem., 38 (1995) 1974–1989.

[86] Horwitz, J.P., Massova, I., Wiese, T.E., Besler, B.H. and Corbett, T.H., Comparative molecular field analysis of the antitumor activity of 9H-

thioxanthen-9-one derivatives against pancreatic ductal carcinoma 03, J. Med. Chem., 37 (1994) 781–786, 3196.

[87] Horwitz, J.P., Massova, I., Wiese, T.E., Wozniak, A.J., Corbett, T.H., Seboltleopold, J.S., Capps, D.B. and Leopold, W.R., Comparative molecular-field analysis of in vitro growth-inhibition of L1210 and HCT-8 cells by some pyrazoloacridines, J. Med. Chem., 36 (1993) 3511–3516.

[88] Jones, J.P., He, M., Trager, W.F. and Rettie, A.E., Three-dimensional quantitative structure–activity relationships for inhibitors of cytochrome P450 2C9, Drug Metab. Disp., 24 (1996) 1–6.

[89] Kellogg, G.E., Kier, L.B., Gaillard, P. and Hall, L.H., E-state fields: Applications to 3D QSAR, J. Comput.-Aided Mol. Design, 10 (1996) 513–520. 129. Kenny, P.W., Prediction of hydrogen bond basicity from computed molecular electrostatic properties: Implications for comparative molecular field analysis, J. Chem. Soc. Perkin Trans., 2 (1994) 199–202.

[90] Kim, K.H., 3D-quantitative structure–activity relationships: Describing hydrophobic interactions directly from 3D structures using a comparative molecular–field analysis (CoMFA) approach, Quant. Struct.-Act. Relat., 12 (1993) 232–238.

[91] Kim, K.H. and Kim, D.H., Description of hydrophobicity parameters of a mixed set from their threedimensional structures, Bioorg. Med. Chem., 3 (1995) 1389–1396.

[92] Kim, K.H., Calculation of hydrophobic parameters directly from their three-dimensional structures using comparative molecular field analysis, J. Comput.-Aid. Mol. Design, 9 (1995) 308–318.

[93] Kim, K.H., Nonlinear dependence in comparative molecular field analysis (CoMFA), J. Comput.-Aid. Mol. Design, 7 (1993) 71–82.

[94] Kim, K.H., Separation of electronic, hydrophobic, and steric effects in 3D-quantitative structure– activity relationships with descriptors directly from 3D structures using a comparative molecular field analysis (CoMFA) approach, Current Topics Med. Chem., 1 (1993) 453–467.

[95] Kim, K.H., Use of indicator variable in comparative molecular field analysis, Med. Chem. Res., 3 (1993) 257 -267.

[96] Kim, K.H., Greco, G., Novellino, E., Silipo, C. and Vittoria, A., Use of the hydrogen bond potentialfunction in a comparative molecular field analysis (CoMFA) on a set of benzodiazepines, J. Comput. Aid. Mol. Deign, 7 (1993) 263–280.

[97] Kimura, T., Miyashita, Y., Funatsu, K. and Sasaki, S.-i., Quantitative structure–activity relationships of the synthetic substrates for elastase enzyme using nonlinear partial least squares regression, J. Chem. Inf. Comput. Sci., 36 (1996) 185–189.

[98] Kireev, D.B., Chretien, J.R. and Raevsky, O.A., Molecular modeling and quantitative structure– activity studies of anti-HIV-1 2-heteroarylquinoline-4-amines, Eur. J. Med. Chem., 30 (1995) 395–402.

[99] Klebe, G. and Abraham, U., On the prediction of binding properties of drug molecules by comparative molecular field analysis, J. Med. Chem., 36 (1993) 70–80.

[100] Klebe, G., Abraham, U. and Mietzner, T., Molecular similarity indices in a comparative analysis (CoMSIA) of drug molecules to correlate and predict their biological activity, J. Med. Chem., 37 (1994) 4130–4146.

[101] Kneubuhler, S., Thull, U., Altomare, C., Carta, V., Gaillard, P., Carrupt, P.-A., Carotti, A. and Testa, B., Inhibition of monoamine oxidase-B by 5H-Indeno[1,2-c]pyridazines: Biological activities, quantitative structure–activity relationships (QSARs) and 3D-QSARs, J. Med. Chem., 38 (1995) 3874–3883.

[102] Kopponen, P., Sinkkonen, S., Poso, A., Gynther, J. and Karenlampi, S., Sulfur analogues of polychlorinated dibenzo-p-dioxins, dibenzofurans and diphenyl ethers as inducers of CYP1A1 in mouse hepatoma cell culture and structure–activity relationships, Env. Toxicol. Chem., 13 (1994) 1543–1548.

[103] Kroemer, R.T. and Hecht, P., A new procedure for improving the predictiveness of CoMFA models and its application to a set of dihydrofolate reductase inhibitors, J. Comput.-Aid. Mol. Design, 9 (1995) 396–406.

[104] Kroemer, R.T. and Hecht, P., Replacement of steric 6-12 potential-derived interaction energies by atom-based indicator variables in CoMFA leads to models of higher consistency, J. Comput.-Aid. Mol. Design, 9 (1995) 205–212.

[105] Kroemer, R.T., Ettmayer, P. and Hecht, P., 3D-Quantitative structure–activity relationships of human immunodeficiency virus type-1 proteinase inhibitors:

Comparative molecular field analysis of 2-heterosubstituted statine derivatives - implications for the design of novel inhibitors, J. Med. Chem., 38 (1995) 4917–4928.

[106] Kroemer, R.T., Hecht, P. and Liedl, K.R., Different electrostatic descriptors in comparative molecular field analysis: A comparison of molecular electrostatic and Coulomb potentials, J. Comput. Chem., 17 (1996) 1296–1308.

[107] McNaught, K.S.P., Thull, U., Carrupt, P.-A., Altomare, C., Cellamare, S., Carotti, A., Testa, B., Jenner, P. and Marsden, C.D., Effects of isoquinoline derivatives structurally related to 1-methyl-4-phenyl 1,2,3,6-tetrahydropyridine (MPTP) on microchondrial respiration, Biochem. Pharmacol., 51 (1996) 1503–1511.

[108] Medvedev, A.E., Ivanov, A.S., Veselovsky, A.V., Skvortsov, V.S. and Archakov, A.I., QSAR analysis of indole analogues as monoamine oxidase inhibitors, J. Chem. Inf. Comput. Sci., 36 (1996) 664–671.

[109] Merz, A. and Folkers, G., Contribution of electrostatic energies to the CoMFA analysis of herpes simplex virus thimidine kinase inhibitors, J. Mol. Graphics, 12 (1994) 75–76.

[110] Minor, D.L., Wyrick, S.D., Charifson, P.S., Watts, V.J., Nichols, D.E. and Mailman, R.B., Synthesis and molecular modeling of 1-phenyl-1,2,3,4-tetrahydroisoquinolines and related 5,6,8,9-tetrahydro- 13bH-dibenzo[a,h]quinolizines as D1 dopamine antagonists, J. Med. Chem., 37 (1994) 4317–4328.

[111] Navajas, C., Kokkola, T., Poso, A., Honka, N., Gynther, J. and Laitinen, J.T., A rhodopsin-based model for melatonin recognition at its G protein-coupled receptor, Eur. J. Pharmacol., 304 (1996) 173–183.

[112] Navajas, C., Poso, A., Tuppurainen, K. and Gynther, J., Comparative molecular field anlaysis (CoMFA) of MX compounds using different semi-empirical methods: LUMO field and its correlation with mutagenic activity, Quant. Struct.-Act. Relat., 15 (1996) 189–193.

[113] Nayak, V.R. and Kellogg, G.E., Cyclodextrin-barbiturate inclusion complexes: A CoMFA/HINT 3-D QSAR study, Med. Chem. Res., 3 (1994) 491–502.

[114] Nicklaus, M.C., Ford Jr., H.F., Hegedus, L., Milne, G.W.A. and Kelley, J.A., Comparative molecular field analysis of hydrophobicity descriptors of cytosine nucleosides, Quant. Struct.-Act. Relat., 14 (1995) 335–343.

[115] Nordvall, G., Sundquist, S., Johansson, G., Glas, G., Nilvebrant, L. and Hacksell, U., 3-(2-benzofuranyl) quinuclidin-2-ene derivatives: Novel muscarinic antagonists, J. Med. Chem., 39 (1996) 3269–3277.

[116] Norinder, U., A PLS QSAR anlaysis using 3D generated aromatic descriptors of principal property type: Application to some dopamine D2 benzamide antagonists, J. Comput.-Aid. Mol. Design, 7 (1993) 671–682.

[117] Norinder, U., Single and domain model variable selection in 3D QSAR applications, J. Chemomet., 10 (1996) 95–105.

[118] Novellino, E., Fattorusso, C. and Greco, G., Use of comparative molecular field analysis and cluster analysis in series design, Pharm. Acta Helv., 70 (1995) 149–154.

[119] Ohta, M., Koga, H., Sato, H. and Ishizawa, T., Comparative molecular field analysis of benzopyran-4- carbothioamide potassium channel openers, Bioorg. Med. Chem. Lett., 4 (1994) 2903–2906.

[120] Oprea, T.I. and Garcia, A.E., Three-dimensional quantitative structure–activity relationships of steroid aromatase inhibitors, J. Comput.-Aid. Mol. Design, 10 (1996) 186–200.

[121] Oprea, T.I., Waller, C.L. and Marshall, G.R., 3D-QSAR of human immune deficiency virus (I) protease inhibitors: 3. Interpretation of CoMFA results, Drug Des. Discovery, 12 (1994) 29–51.

[122] Oprea, T.I., Waller, C.L. and Marshall, G.R., Three-dimensional quantitative structure–activity relationship of human immunodeficiency virus (I) protease inhibitors: 2. Predictive power using limited exploration of alternate binding modes, J. Med. Chem., 37 (1994) 2206–2215.

[123] Poso, A, Juvonen, R. and Gynther, J., Comparative molecular field analysis of compounds with CYP2A5 binding affinity, Quant. Struct.-Act. Relat., 14 (1995) 507–511.

[124] Poso, A., Tuppurainen, K. and Gynther, J., Modeling of molecular mutagenicity with comparative molecular field analysis (CoMFA): Structural

and electronic properties of MX compounds related to TA100 mutagenicity, J. Mol. Struct. (Theochem), 304 (1994) 255–260.

[125] Poso, A., Tuppurainen, K. and Gynther, J., Molecular genotoxicity of MX compounds and the correlation with LUMO: Comparative molecular field analysis, J. Mol. Graphics, 12 (1994) 70.

[126] Poso, A., Tuppurainen, K., Ruuskanen, J. and Gynther, J., Binding of some dioxins and dibenzofurans to the Ah receptor: A QSAR model based on comparative molecular field analysis (CoMFA), J. Mol. Struct. (Theochem), 282 (1993) 259–264.

[127] Prendergast, K., Adams, K., Greenlee, W.J., Nachbar, R.B., Patchett, A.A., and Underwood, D.J., Derivation of a 3D pharmacophore model for the angiotensin-II site one receptor, J. Comput.-Aided Mol. Design, 8 (1994) 491-512.

[128] Raghavan, K., Buolamwini, J.K., Fesen, M.R., Pommier, Y., Kohn, K.W. and Weinstein, J.N., Threedimensional quantitative structure–activity relationship (QSAR) of HIV integrase inhibitors: A comparative molecular field analysis (CoMFA) study, J. Med. Chem., 38 (1995) 890–897.

[129] Steinmetz, W.E., A CoMFA analysis of selected physical properties of amino acids in water, Quant. Stlruct.-Act. Relat., 14 (1995) 19–23.

[130] Steinmetz, W.E., A CoMFA model of steric and electronic effects of phosphorus ligands, Quant. Struct.-Act. Relat., 15 (1996) 1–6.

[131] Tafi, A., Anastassopoulou, J., Theophanides, T., Botta, M., Corelli, F., Massa, S., Artico, M., Costi, R., Santo, R.D. and Ragno, R., Molecular modeling of azole antifungal agents active against Candida albicans :1. A comparative molecular field analysis study, J. Med. Chem., 39 (1996) 1227–1235.

[132] Waller, C.L. and marshall, G.R., 3-dimensional quantitative structure–activity relationship of angiotensin-converting enzyme and thermolysin inhibitors: 2. A comparison of CoMFA models incorporating molecular-orbital fields and desolvation free-energies based on active-analog and complementary-receptor field alignment rules., J. Med. Chem., 36 (1993) 2390–2403.

[133] Waller, C.L. and McKinney, J.D., Three-dimensional quantitative structure–activity relationships of dioxins and dioxin-like compounds: Model validation and Ah receptor characterization, Chem. Res. Toxicol., 8 (1995) 847–858.

[134] Waller, C.L., Evans, M.V. and McKinney, J.D., Modeling the cytochrome P450-mediated metabolism of chlorinated volatile organic compounds, Drug Metab. Dispos., 24 (1996) 203–210.

[135] Waller, C.L., Minor, D.L. and McKinney, J.D., Using three-dimensional quantitative structure–activity relationships to examination of the estrogen-receptor binding affinities of polychlorinated hydroxybiphenyls using three-dimensional quantitative structure–activity relationships, Environ. Health Perspect., 103 (1995) 702–707.

[136] Waller, C.L., Oprea, T.I., Chae, K., Park, H.-K., Korach, K.S., Laws, S.C., Wiese, T.E., Kelce, W.R. and Gray, Jr., L.E., Ligand-based identification of environmental estrogens, Chem. Res. Toxicol., 9 (1996) 1240–1248.

[137] Waller, C.L., Oprea, T.I., Giolitti, A. and Marshall, G.R., Three-dimensional QSAR of humanimmunodeficiency- virus-I protease inhibitors: 1. A CoMFA study employing experimentally determined alignment rules, J. Med. Chem. 36 (1993) 4152–4160.

[138] Waller, C.L., Wyrick, S.D., Kemp, W.E., Park, H.M. and Smith, F.T., Conformational-analysis,molecular modeling, and quantitative structure–activity relationship studies of agents for the inhibition of astrocytic chloride transport, Pharm. Res., 11 (1994) 47–53.

[139] Cho, S.J. and Tropsha, A., Cross-validated R2-guided region selection for comparative molecular field analysis: A simple method to achieve consistent results, J. Med. Chem., 38 (1995) 1060–1066.

[140] Viswanadhan, V.N., Ghose, A.K., Revankar, G.R. and Robins, R.K., Atomic physicochemical parameters for 3 dimensional structure directed quantitative structure activity relationships. 4. Additional parameters for hydrophobic and dispersive interactions and their application for an automated superposition of certain naturally-occurring nucleoside antibiotics, J. Chem. Inf. Comput. Sci., 29 (1989) 163–172.

[141] Klebe, G., The use of composite crystal-field environments in molecular recognition and the de novo design of protein ligands, J. Mol. Biol., 237 (1994) 212–235.

[142] Teixeira, C., Serradji, N., Maurel, F. and Barbault, F., Docking and 3D-QSAR studies of BMS-806 analogs as HIV-1 gp120 entry inhibitors, Eur. J. Med. Chem., 44 (2009) 3524–3532.

[143] Wold, S., Sjostrom, M. and Eriksson, L., PLS-regression: a basic tool of chemometrics, Chemom. Intell. Lab. Syst., 58 (2001)109–130.

[144] Kettaneh, N., Berglund, A. and Wold, S., PCA and PLS with very large data sets, Comput. Stat. Data. Anal., 48 (2005) 69–85.

[145] Wold, S., Johansson, E. and Cocchi, M., PLS: Partial Least Squares Projections to Latent Structures. In: 3D QSAR in Drug Design: Theory, Methods and Applications, ESCOM Science Publishers, Leiden, 1993, pp. 523-550.

[146] Spoel, D.V., Lindahl, E., Hess, B., Groenhof, G., Mark, A.E. and Berendsen, H.J.C., GROMACS: Fast, Flexible, and Free., J. Comput. Chem., 26 (2005) 1701–1718.

[147] Schuettelkopf, A.W. and van Aalten, D.M.F., PRODRG - a tool for high-throughput crystallography of protein–ligand complexes, Acta. Crystallogr. Biol. Crystallogr., D60 (2004) 1355–1363.

[148] Parrinello, M. and Rahman, A., Polymorphic transitions in single crystals: A new molecular dynamics method, J. Appl. Phys., 52 (1981) 7182–7190.

[149] Essmann, U., Perera, L., Berkowitz, M., Darden, T., Lee, H., and Pedersen, L., A smooth particle mesh Ewald method, J. Chem. Phys., 103 (1995) 8577–8593.

[150] Lin, J.H., Perryman, A.L., Schames, J.R. and McCammon, J.A., Computational drug design accommodating receptor flexibility: The relaxed complex scheme, J. Am. Chem. Soc., 124 (2002) 5632–5633.

[151] Marriott, D.P., Dougall, I.G., Meghani, P., Liu, Y.J. and Flower, D.R., Lead generation using pharmacophore mapping and threedimensional database searching: application to muscarinic M (3) receptor antagonists, J. Med. Chem., 42 (1999) 3210–3216.

[152] Talele, T.T., Kulkarni, S.S. and Kulkarni, V.M., Development of pharmacophore alignment models as input for comparative molecular field analysis of a diverse set of azole antifungal agents, J. Chem. Inf. Comput. Sci., 39 (1999) 958–966.

[153] Karki, R.G. and Kulkarni, V.M., A feature based pharmacophore for Candida albicans MyristoylCoA: protein N-myristoyltransferase inhibitors, Eur. J. Med. Chem., 36 (2001) 147–163.

[154] Hurst T., Flexible 3D searching - the directed tweak technique, J. Chem. Inf. Comput. Sci., 34 (1994) 190–196.

[155] Jain, A.N., Surflex: Fully Automatic Flexible Molecular Docking Using a Molecular Similarity-Based Search Engine, J. Med. Chem., 46 (2003) 499–511.

[156] Jain, A.N., Virtual screening in lead discovery and optimization, Curr. Opin. Drug. Discov & Devel., 7 (2004)396–403.

[157] Jain, A.N., Scoring noncovalent protein-ligand interactions: a continuous differentiable function tuned to compute binding affinities, J. Comput. Aided. Mol. Des., 10 (1996) 427–440.

[158] Jain, A.N., Scoring functions for protein-ligand docking, Curr. Protein. Pept. Sci., 7 (2006) 407–420.

[159] Golbraikh, A., and Tropsha, A., Beware of q2, J. Mol. Graph. Model., 20 (2002) 269–276.

Appendix

Appendix A

Acknowledgments

The completion of my doctoral studies would not have been possible without the help of many people. First of all, I would like to express my sincere gratitude to my advisor respected **Prof. Seung Joo Cho**, for his love, guidance, patience, support and friendship both professionally and personally during the entire course of this dissertation. He has been a wonderful guide, providing me with the best working ambience and continuous support. His overly enthusiasm and integral view on research and his mission for providing 'only high-quality work and not less', has made a deep impression on him. I owe him lots of gratitude for having me shown this way of research. He could not even realize how much I have learned from him. I am really glad that I have met you in my life Sir.

I take this opportunity to thank **Prof. Honglae Sohn** in department of chemistry for his great guidance and instruction in scientific area. Many thank him accepting to be the chair of the graduation committee.

I would like to extend my warm thanks to **Dr.Sharmistha Dey, Antony Martin**, **Dr.Balachandran**, and **Sharein** for their wonderful support and motivation for my life.

I would also like to thank to my fellow graduate students that I have worked with **Gugan, Sungyong Um**, **Sung-Gi Lee**, **Bo-Yeon Lee**, **Min Woo Hwang**, **Hyun Cho**, their cooperation and help to my research.

The chain of my gratitude would be definitely incomplete if I would forget to thank my friends **Venkat**, **Karthi**, **Ganesh babu**, **Kumaresan**, **Rao**, **Niyaz**, **Sathish**, **Kalai**, **Vedamalai**, **Muniaswamy**, **Bijoy**, **Changdev, Gopal**, **Rajesh**, **Merlin,** all my school friends, Chosun university friends, and all my Korean friends, Words just cannot describe the help they have done to me. The true spirit and force of my life has always been your love and friendship, and will always be.

I thank my beloved **Durgadevi** (mother), **Pushpalatha** (sister), **Suresh** (brother), **logesh, and** A**jay** for their love and support during all walks of my life. My sister and mother have always been extremely patient, tirelessly supportive and words cannot describe what they have been to me throughout my life. Their blessings have helped me to become what I am today. Last, but not the least, I offer my humble salutations to GOD for everything.

This thesis is dedicated to all of them.

Appendix B

List of Publication

1. **Madhavan T**, Chung JY, Kothandan G, Gadhe CG, Cho SJ. 3D-QSAR Studies of JNK1 Inhibitors Utilizing Various Alignment Methods. *Chem Biol Drug Des*. **(in press)** (2011).
2. **Madhavan T**, Gadhe CG, Kothandan G, Lee K, Cho SJ. Various Atomic Charge Calculation Schemes of CoMFA on HIF-1 Inhibitors of Moracin Analogs. *Int J Quantum Chem* (in press DOI: 10.1002/qua.23084) (2011)
3. **Madhavan T**, Kothandan G, Gadhe CG, Cho SJ. QSAR analysis on PfPK7 inhibitors using HQSAR, CoMFA, and CoMSIA. *Med Chem Res.* (in press DOI: 10.1007/s00044-011-9572-x) (2011)
4. Gadhe CG, **Madhavan T**, Kothandan G, Cho SJ. In Silico Quantitative Structure-Activity Relationship Studies on P-gp Modulators of Tetrahydroisoquinoline-Ethyl-Phenylamine Series. *BMC Structural Biology* 11: 1-15 (2011)
5. Kothandan G, Gadhe CG, **Madhavan T**, Cho SJ. Binding Site Analysis of CCR2 Through In Silico Methodologies: Docking, CoMFA, and CoMSIA. *Chem Biol Drug Des*.78: 161-174 (2011).
6. Kothandan G, Gadhe CG, **Madhavan T**, Cho SJ. Docking and 3D-QSAR (quantitative structure activity relationship) studies of flavones, the potent inhibitors of p-glycoprotein targeting the nucleotide binding domain. *Eur J Med Chem.* (in press DOI: 10.1016/j.ejmech.2011.06.008)
7. Gadhe CG, **Madhavan T**, Kothandan G, Lee TB, Lee K, Cho SJ. Various Partial Charge Schemes on 3D-QSAR Models for P-gp Inhibiting Adamantyl Derivatives. *Bull Korean Chem Soc*. 32: 1604-1612 (2011)
8. Gadhe CG, Lee SH, **Madhavan T**, Kothandan G, Choi DB, Cho SJ. Ligand Based CoMFA, CoMSIA and HQSAR Analysis of CCR5 Antagonists. *Bull Korean Chem Soc*. 31: 2761-2770 (2010).

9. Gadhe CG, Kothandan G, **Madhavan T**, Cho SJ. Molecular modeling study of HIV-1 gp120 attachment inhibitors. *Med Chem Res*. (in press DOI: DOI 10.1007/s00044-011-9711-4)
10. Singh AK, Parshad R, Pasi S, **Madhavan T,** Das SN, Mishra B, Gill K, Dalal K, Dey S. Prognostic Significance of Cyclooxygenase-2 and Response to Chemotherapy in Invasive Ductal Breast Carcinoma Patients by Real Time Surface Plasmon Resonance Analysis. DNA Cell Biol. (in press DOI: 10.1089/dna.2011.1215)